Aerodynamic Drag Reduction of Commercial Trucks

Cheng Wang

April 2000

Submitted In Partial Fulfilment

For The Degree of Master of Science In The

Department of Mechanical Engineering

University of Cape Town

DECLARATION

I, Cheng Wang, hereby declare that this dissertation is my own work and it is being submitted for the degree of Master of Science in Engineering at the University of Cape Town. This work has not previously been submitted for any degree at any university.

Signed by candidate

Date: 28. 04. 2000

Signature removed

ACKNOWLEDGEMENTS

The author is grateful to Prof. A. T. Sayers for his valuable time and the kind supervision of this work. Thanks are also addressed to Dr. H. Pearce for his support on the numerical work. The author would like to thank the departmental and workshop staff, as well as my fellow students, for being always friendly and helpful in virtually every aspect.

SYNOPSIS

This thesis deals with the airflow over a double trailer Gull Wing truck, with a view to reducing the drag of the truck. To investigate the flow over the truck, a 1:20 scale double trailer truck model was designed and constructed from chipboard for wind tunnel experiments. The overall size of the model is 1100 mm long, 130 mm wide and 215 mm high. A same scale numerical model was also built for computational simulations.

A series of wind tunnel tests were carried out in a low speed wind tunnel to investigate the aerodynamic drag on the double-trailer model truck. Numerous add-on devices were designed for reducing drag. To assess the effectiveness of these devices, drag forces and pressure distributions on the surfaces of the trailers were measured with and without the devices attached. The drag tests were carried out at yaw angles of 0^0 and 5^0 and Reynolds numbers ranging from 0.94×10^5 to 2.59×10^5 based on the overall width of the model. Tests for measuring the pressure distributions were conducted at a Reynolds number of 1.6×10^5 and zero yaw. Flow visualization studies with cotton tufts were conducted to highlight details of the flow.

The air deflection add-on devices include a cab roof deflector, centre and side gap seals, side skirts and some rear face fairings. End guide vanes, cavities, edge fairings and a rear fender are described as rear face fairings. All the add-on devices mounted on the basic truck model were tested on their own or in a combination with other add-on devices.

The results obtained from the wind tunnel experiments indicate that at a Reynolds number of 1.6×10^5, a reduction in drag coefficient of approximately 30% was achieved at both 0^0 and 5^0 yaw angles. The drag increase or decrease caused by fitting rear face fairings lay within $\pm$ 7% depending upon the

fitting concerned. Side gap seals are more effective in drag reduction at a yaw angle and, have a profound influence on the flow under the truck body, especially in crosswind conditions. A center gap seal has no effect on under-body flow of a truck. For all the models tested in the wind tunnel experiments, their drag coefficients did not vary with Reynolds numbers above 1.65×10^5 at both 0^0 and 5^0 yaw angles.

The 2-dimensional simulations of the airflow over the basic truck model and models with some add-on devices were performed with the CFD program – Flo++. Due to the high ground clearance of the truck, the pressure distribution on the rear face of the rear trailer is symmetric about the horizontal centre line of the face.

From the results of both wind tunnel tests and CFD simulations, it is suggested that for a future commercial truck design, the gap between the cab and trailer should be removed.

TABLE OF CONTENTS

NOMENCLATURE

A	frontal projected area of truck (H x W), m^2
C_D	drag coefficient (= $D/0.5\rho V^2 A$)
C_P	pressure coefficient { = $(P-P_\infty)/0.5\rho V^2$ }
D	drag force in body system, N
D_m	measured drag force in free stream direction, N
H	overall height of model, m
P	static pressure, Pa
P_∞	static atmospheric pressure, Pa
R_e	Reynolds number (= VW/ν)
U	velocity vector, m/s
V	free stream velocity, m/s
W	total width of the model, m
u, v, w	velocity components in Cartesian coordinates, m/s
x, y, z	Cartesian coordinates, m

Greek

ρ	free stream density, kg/m^3
ν	kinematic viscosity, m^2/s
μ	dynamic viscosity, N s/m^2
β	yaw angle, degrees
τ_{ii}	shear force in the i direction on the ii plane, N/m^2
τ_{ij}	shear force in the j direction on the ij plane, N/m^2

Subscripts

0	refers to basic truck without drag reduction devices

CHAPTER 1 - INTRODUCTION

The reduction of drag force on commercial trucks has been of interest to engineers and researchers for many years, with a view to saving fuel. This is based on the fact that fuel consumption takes up about 50 percent of the daily operational cost for commercial trucks [1] and, a significant decrease in fuel consumption could be achieved by improving the aerodynamics of the truck. Under heavily competitive conditions, keeping the daily operational costs as low as possible will help to maintain the relevant company in a favourable economic position.

For an existing basic commercial truck, the aerodynamic drag is usually reduced by means of an appropriate device mounted on it. Some practical devices for this purpose have been successfully developed and used on some commercial trucks in daily operation, and typically consist of cab roof mounted deflectors and container forebody fairings. However, it is worth noting that there are still a large proportion of commercial trucks running without any aerodynamic treatment, especially those with a large gap between the cab and trailer. Compared to trains, cars and other transport vehicles, there has been little change to the external shapes of commercial trucks to improve their aerodynamic characteristics. This implies that further research on the aerodynamic characteristics of trucks is needed, for the development of new and effective practical devices for drag reduction.

Wind tunnel experiments are the most common means of studying the aerodynamic behavior of a vehicle. They are characterized by a scaled model being at rest in a wind tunnel and the air blowing against the model. The aerodynamic forces and moments experienced by the model are measured by

means of a balance in connection with the model. The pressure distributions on the various surfaces of the model are usually measured through pressure tappings connected to a manometer.

Usually three orthogonal forces, namely, lift, drag and side force, are used to describe the aerodynamic characteristics of a body. In the case of commercial trucks, the drag is of primary significance. Therefore, for all the models with or without drag reduction devices examined in this research, only this parameter is considered.

Another useful and powerful tool for the investigation of airflow over a truck is computational studies. Some commercial Computational Fluid Dynamics (CFD) codes have been developed and used in the study of vehicle aerodynamics. To simulate the airflow over a commercial truck with a computer, a mathematical model is defined using the governing equations. After setting the relevant boundary conditions according to the running condition of the truck on the road, the governing equations are then solved by numerical schemes, such as finite element, finite volume or finite difference techniques.

Compared to experimental methods, computer studies have some obvious advantages. For example, with a computer, simulation of the relative motion between the vehicle and road is comparatively easy to achieve. Also the blockage effect due to the size of the model in the wind tunnel can be eliminated through setting a large enough computational space. However, the experimental testing should not be completely substituted by the computational simulations because of limitations of the numerical method itself. Since the configuration of a commercial truck is very complicated, it is not always easy to include adequate details of the truck geometry in a computational study.

Usually, a simplified geometric profile of a truck is presented in numerical modelling.

The object of this thesis is to investigate the aerodynamic drag on a South African Breweries (S.A.B.) double trailer Gull Wing truck, and to identify and quantify regions on the truck responsible for high drag losses through both wind tunnel tests and CFD studies. Based on analyzing the aerodynamic characteristics of the truck, some design recommendations for the practical reduction of the aerodynamic drag are made. Some add-on devices are designed and constructed for drag reduction. Through pressure distributions on the trailer surfaces, the effectiveness of the devices are assessed. Possible future designs for a commercial truck in tractor-trailer combinations are also suggested.

The thesis begins with a comprehensive literature survey, in which various techniques for reducing truck aerodynamic drag are discussed. In Chapter 3, wind tunnel experiments with a scaled model of the double trailer truck are presented. Experimental results are presented and discussed in Chapter 4. Chapter 5 deals with the computational (CFD) simulation for the airflow over some models of the truck. Finally, conclusions relating to the aerodynamic drag reduction of commercial trucks are drawn in Chapter 6.

CHAPTER 2 - LITERATURE SURVEY

In this chapter, the most important aspects concerning drag reduction of commercial trucks are discussed in a comprehensive literature review. Besides a great number of SAE (Society of Automotive Engineers) papers that deal with this topic, some other papers about the issue were also found in relevant journals and books. Accordingly, the aspects analyzed in this chapter have the following structure:

- Fuel consumption of commercial trucks
- Geometric characteristics of a commercial truck
- Aerodynamic characteristics of a commercial truck
- Drag reduction techniques
- Wind tunnel experiments
- Numerical methods

2.1 FUEL CONSUMPTION OF COMMERCIAL TRUCKS

The fuel of a commercial truck is usually consumed to overcome aerodynamic drag, rolling resistance, breaking and transmission losses. Since the aerodynamic drag is a function of the square of the truck velocity, it plays an important role in the fuel consumption and operational cost for commercial trucks running at higher speeds. In general, at higher speeds, almost 50-70 percent of the fuel consumption of a commercial truck is due to overcoming the aerodynamic drag [2, 3]. From Fig. 2.1, it is clearly seen that at speeds greater than 40 mph, the fuel cost increases rapidly, and the drag coefficient of a truck has a great effect on the cost per mile [1].

Through aerodynamic improvements to commercial trucks, a considerable reduction in aerodynamic drag can be obtained, consequently resulting in a significant increase in profits. For example, a 50% increase in profits is achieved when there is a 15% reduction in aerodynamic drag on a commercial truck [1].

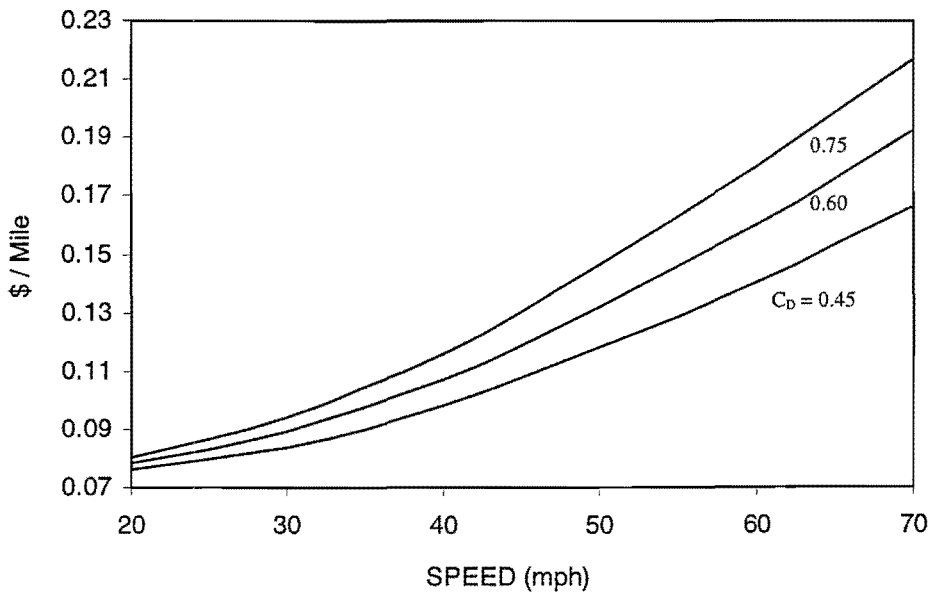

Fig. 2.1: Cost per mile versus vehicle speed (no wind)

The following simple equation (1) can be applied to assess the significance of the reduction in aerodynamic drag in terms of fuel consumption [4].

$$\text{Fuel Saving}\,(\%) = \text{Drag Reduction}\,(\%)\frac{\text{Air Drag Power}}{\text{Total Power}} \qquad (1)$$

For a particular commercial truck, the air drag power varies with the weight of the tractor-trailer combination and the truck cruising speed.

2.2 GEOMETRIC CHARACTERISTICS OF A COMMERCIAL TRUCK

A commercial truck is typically in a form of one tractor and one trailer while some heavy trucks have one tractor and two trailers. Since the load carrying capacity is of utmost importance, the trailer is consequently constructed in a box shape in order to maximize the effective volume within legal limits. In contrast with trailers, the truck cab has more freedom in its external shape. Usually the trailer is higher and wider than the tractor. According to Mason and Beebe [5], a typical profile of a commercial truck shown in Fig. 2.2 demonstrates the geometric characteristics, where an effective diameter based on the projected frontal area is used.

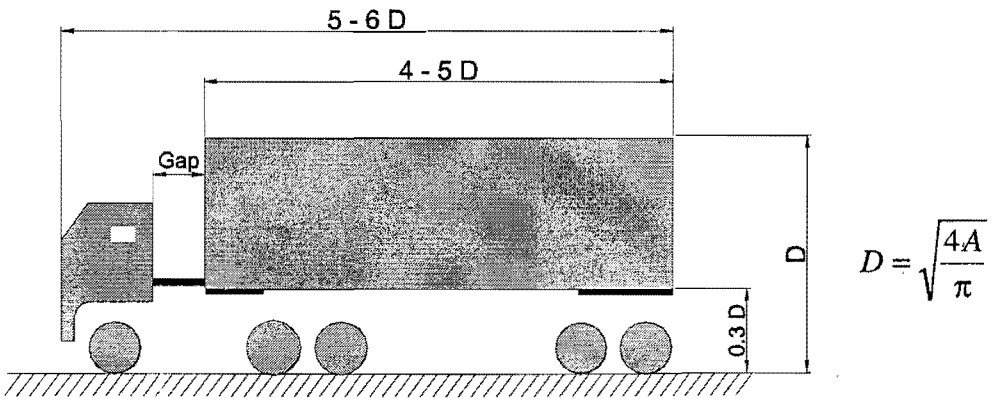

Fig. 2.2: Profile of a typical truck

The gap between cab and trailer is commonly within the range of 0.3 - 0.6 D, which provides the truck with small-radius turning. The aspect ratio of the trailer cross-section is unity. Normally the ground clearance of the trailer is constant and equal to about 0.3 D.

2.3 AERODYNAMIC CHARACTERISTICS OF A COMMERCIAL TRUCK

The aerodynamic characteristics of a commercial truck are determined by its geometric characteristics. From the aerodynamic point of view, a commercial truck is typically a bluff body, and as a result the drag on it is mainly pressure drag [6]. Special attention should be paid to three important features of the airflow over commercial trucks.

- **Two stagnation points**

As air blows against a truck, two stagnation points on the truck body can be observed: one on the frontal face of the cab and another on the exposed front face of the trailer due to the difference between heights of tractor and trailer, as shown in Fig. 2.3a. The second stagnation point causes an increase in total pressure on the front vertical face of the trailer, resulting in a considerable increase in drag on the truck.

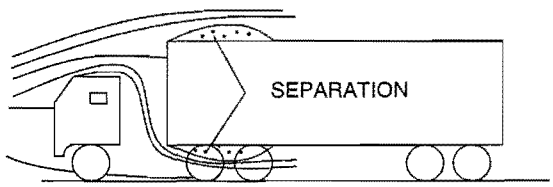

a: side view

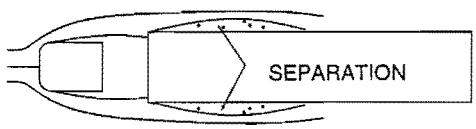

b: top view

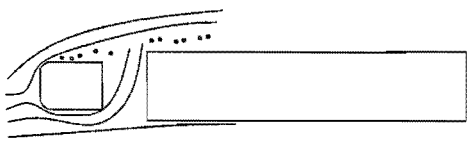

c: top view, yawed truck

Fig. 2.3: Flow separation on a truck

- **Separation at the forward edges of trailers**

A substantial part of the aerodynamic drag on a commercial truck is that caused by the flow separation that occurs at the forward edges of the trailer. For a cab-over-engine truck moving in still air, this drag may amount to as much as one third of the total aerodynamic drag [7].

The flow separation increases the drag on trucks by increasing the average pressure acting on the front vertical face of the trailer. The situation would be aggravated under the condition of a yaw angle, which is defined as the angle between the direction of travel and the relative wind velocity. This is due to the fact that a cross airflow through the gap between the back of the cab and the trailer worsens the separation at the trailer's leeward edge, seen in Fig. 2.3c.

- **Recirculating flow in the near wake**

The third important feature for the flow around commercial trucks is the flow recirculation in the near wake of trailers. Because a second boundary layer separation occurs at the rear edges of the trailer, a separation bubble is formed in the near wake, shown in Fig. 2.4. For a bluff body there will be two separation bubbles in the wake when it is far from the ground [8, 9]. Mason and Beebe [5] have indicated that on the rear face of the trailer there is a characteristic vertical pressure gradient, and the pressure values are invariant transversely across the face (Fig. 2.5).

2.4 DRAG REDUCTION TECHNIQUES

In terms of the geometric and aerodynamic characteristics of a commercial truck, most drag reduction techniques are accomplished by changing pressures on the front and back surfaces of the trailers or minimizing flow separations.

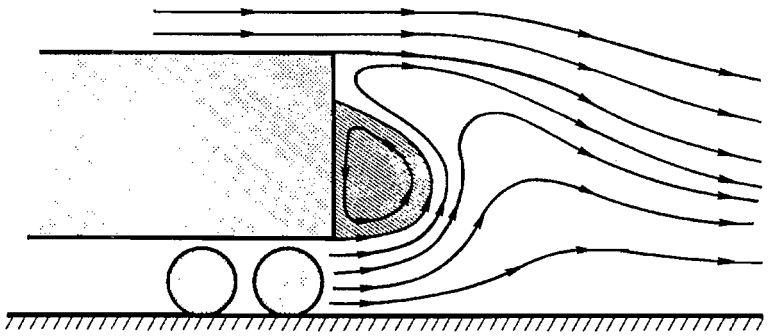

Fig. 2.4: Recirculating flow in the near wake of trailer

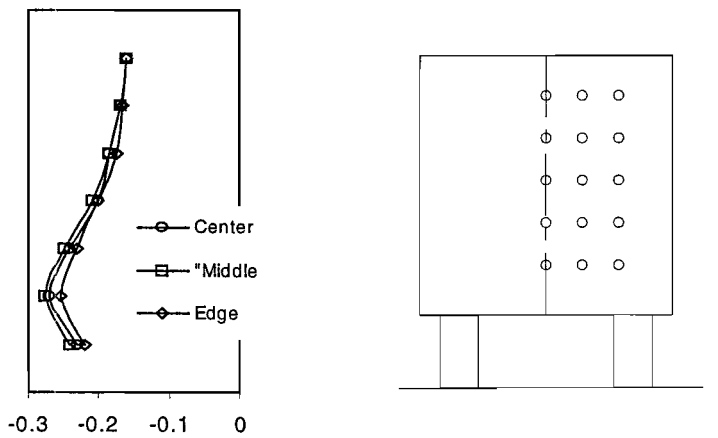

Fig. 2.5: Tractor-trailer base pressure distributions

In general, through modifications to the external shape of a truck, especially by fitting appropriate add-on air deflector devices, the vehicle's aerodynamic characteristics can be significantly improved, which consequently results in a drag reduction.

One direct method to improve the aerodynamic characteristics of trucks is to optimize the cab geometry aerodynamically. Gilhaus [10] has investigated the effect of cab design parameters on the air drag of trucks, and similar work has been done with CFD by Craig et al. [11].

A semipassive drag reduction method is introduced by Modi et al. [12]. On the basis of the concept of a moving boundary-layer, the method uses rotating hollow cylinders to delay separation of the boundary-layer on the top surface of the trailer which reduces the pressure drag. Fig. 2.6 shows the configuration of the model. A drag reduction of 26% was achieved using this technique.

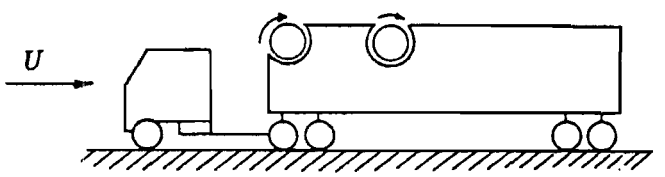

Fig. 2.6: Configuration of a truck model
with rotating cylinders

- **Cab roof deflectors**

A cab roof deflector is one of the most effective drag reduction devices and has been applied widely in day to day operations of commercial trucks. A simple type of cab roof deflector, frequently appearing in research, is a flat plate. The curves of wind averaged drag coefficients vary with a flat plate deflector inclination angle as shown in Fig. 2.7 [3]. Although at zero yaw angle, a flat plate mounted on the cab roof may provide significant drag reduction, the drag may increase at a small yaw angle because of the yaw sensitivity of the truck configuration [13]. Since trucks running on roads invariably experience a yaw angle which is usually less than 5 degrees, a flat plate mounted on the cab roof is not practical as a drag reduction device.

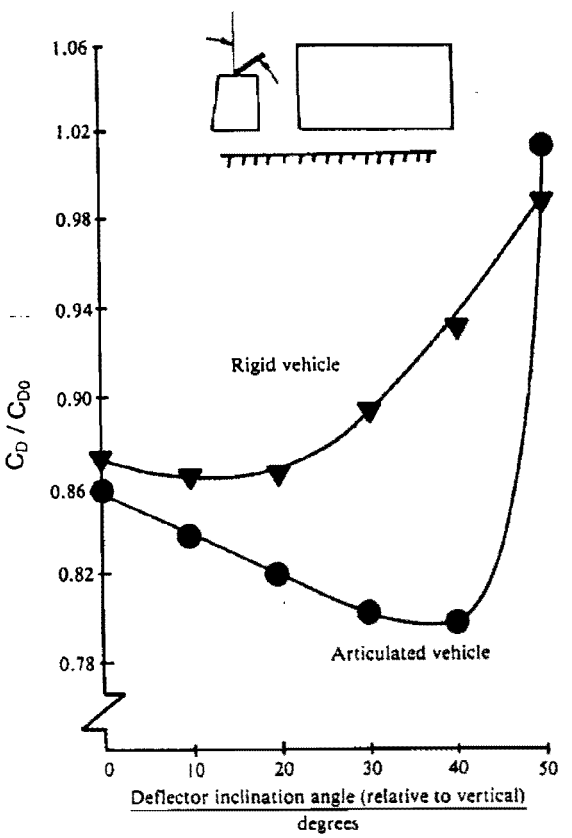

Fig. 2.7: Drag decrease versus deflector inclination angle.

The work of Marks et al. [7] shows that a cab-mounted fairing with both curved top and side surfaces could provide greater drag reductions at all yaw angles in comparison with a fairing which is curved on the top or side surface (Fig. 2.8). Generally, cab roof deflectors are more effective on commercial vehicles with a larger cab-container gap [3]. From Fig. 2.8, it can be seen that the effectiveness of cab mounted fairings is reduced as the yaw angle increases.

By fitting air deflectors on the cab roof, the double-stagnation flow field on trucks can be transformed into a single-stagnation field, like that of buses. Similarly, the flow separation occurring on the trailer foreward edges can also be minimized by fitting deflectors, which also results in the truck's drag being reduced significantly [7].

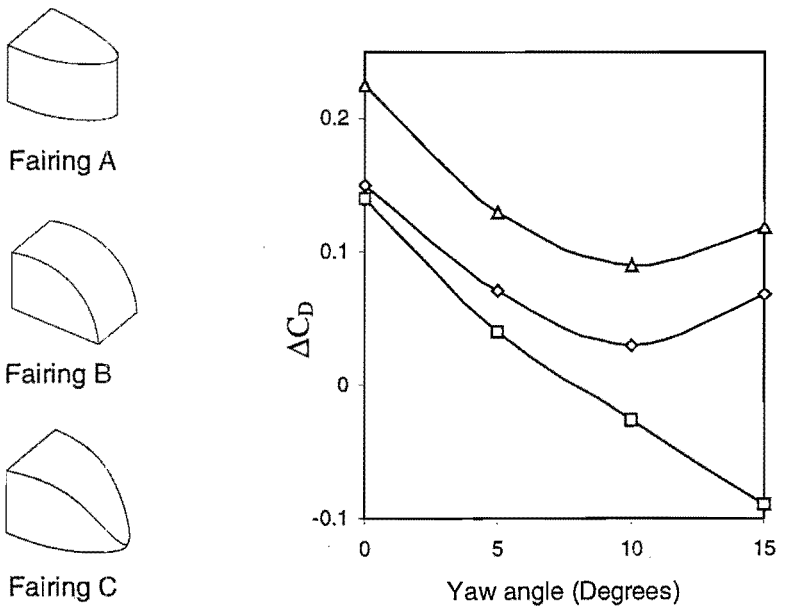

Fig. 2.8: Sketch of three cab roof deflectors and the corresponding decreases in drag coefficient

- **Trailer frontal face fairings**

Trailer frontal face fairings consist of different types, such as bubble-shaped mouldings, guide vanes and edge fairings. Some typical types of trailer frontal face fairings are shown in Fig. 2.9. According to the results of Garry [14], by the addition of the bubble-shaped and edge fairings, drag reductions of about 33% for rigid and 23% for articulated vehicles were obtained at the zero yaw condition. At a yaw angle of 20^0 the corresponding reductions are 21% and 11% respectively.

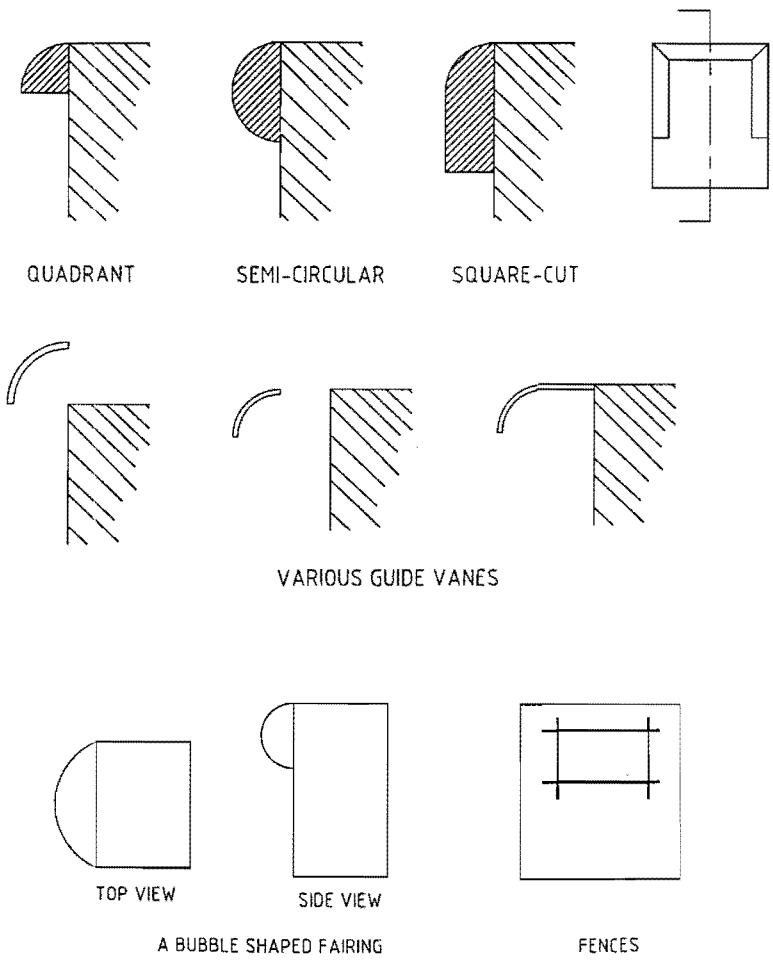

Fig. 2.9: Typical trailer frontal face add-on devices

Modi et al. [2] used fences fitted on the trailer frontal face, as shown in Fig. 2.9, to promote the flow separation, and thereby reduced the pressure drag on the face. For a cube shaped van, maximum reductions of about 31% and 16.6% in the drag coefficient were obtained by means of this method in separate wind tunnel and road tests respectively.

Compared to cab roof deflectors, trailer forebody fairings are more effective on a rigid chassis than on articulated vehicles since they prevent flow separations at the forward edges of the trailer. "In general, well designed container forebody edge fairings, will give larger reductions in wind averaged drag than a roof deflector" [3].

(The concept of a wind-averaged drag coefficient was first introduced by Buckley and Sekscienski [15], and is used to reflect the average level of drag on a truck under national average operating conditions.)

- **Gap seals and cab rear-side fairings**

Gap seals and cab rear-side fairings are not used on their own, but are usually used in conjunction with a cab roof deflector. Both devices are used to prevent flow separation on the forward side edges of the trailer.

When a truck runs under crosswind conditions, there will be a crossflow through the cab-trailer gap, from the windward side to the leeward side of the vehicle because of the pressure difference between them. The crossflow causes a premature flow separation on the leeward side and consequently increases the total drag of the truck. In order to prevent this crossflow, a gap seal, usually in the form of a flat plate is placed vertically along the centre-line of the vehicle between the cab and trailer [7, 16, 17, 18]. A model truck with cab deflector and gap seal is illustrated in Fig. 2.10.

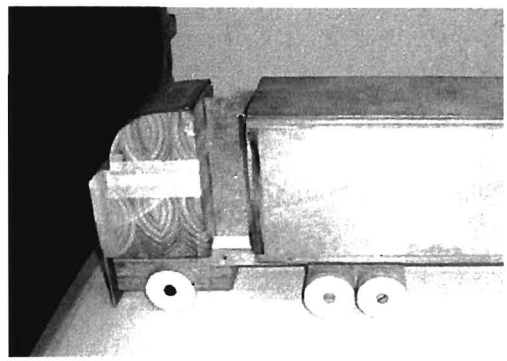

Fig. 2.10: Model with a cab deflector and gap seal

Buckley et al. [18] show that the addition of a gap seal can provide additional drag reduction only at non-zero yaw angles. A model truck with a gap seal is shown in Fig. 2.10. The results of the on-road tests of Buckley et al. [18] indicate that an extra 8% reduction in wind-averaged drag was achieved through fitting a gap seal to the tested truck. In spite of producing a considerable drag reduction, the application of gap seals in practical operations is usually restricted by the manoeuvrability of the truck unit.

A proprietary device called AirTab has also been introduced in commercial truck operations [19]. AirTabs fitted to the rear of the cab can reduce the airflow into the gap between the tractor and trailer and hence reduce the aerodynamic drag of the truck, as shown in Fig. 2.11. Its principle of operation is that a vortex curtain can be created by means of the AirTabs along the two sides of a truck, and this curtain prevents air from entering the gap and creating turbulence (Fig. 2.12). A 4% fuel saving can be achieved by applying AirTabs in commercial truck operations.

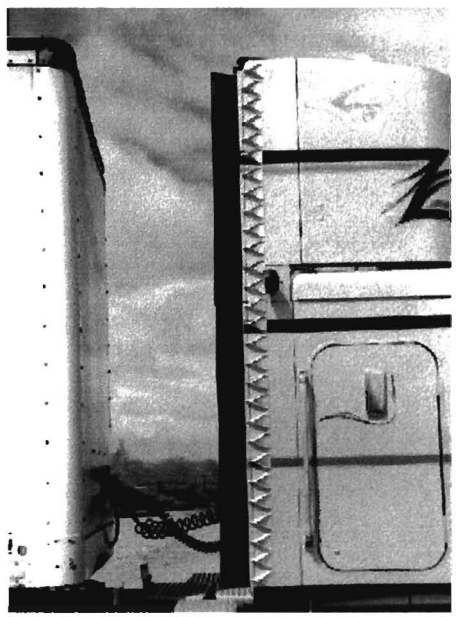

Fig. 2.11: AirTabs added on a truck

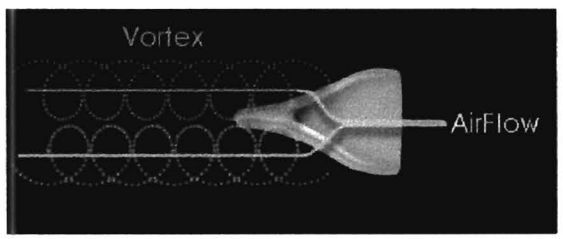

Fig. 2.12: Working principle of an Airtab

For trucks with a wider trailer than the tractor, tractor rear-side fairings are used to reduce the total drag through the improvement of the flow matching between tractor and trailer, as shown in Fig. 2.13. It has been proved that a matched flow field between two bluff bodies leads to a lower level of drag [3, 5]. For a bulk sugar carrier, a drag reduction of 18% was achieved by fitting faired panels on the rear side edges of the tractor [4].

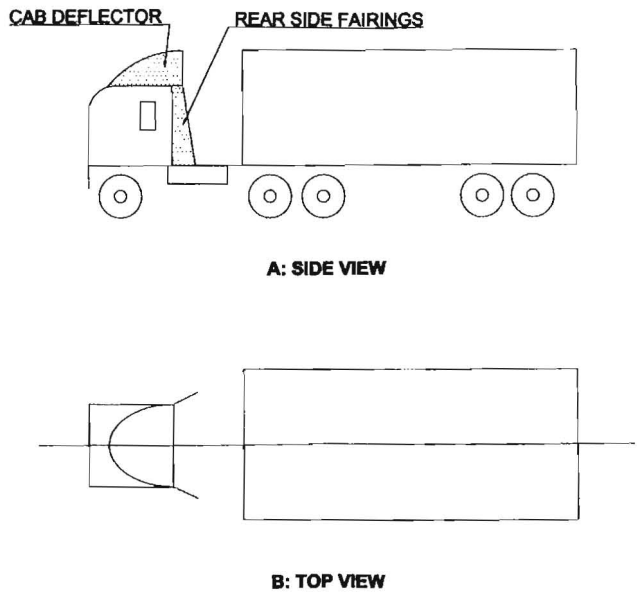

Fig. 2.13: Sketch of a truck with cab rear-side fairings

- **Side skirts**

The underbody flow is considered as one of the main sources contributing to the aerodynamic drag of commercial trucks. Since a commercial truck usually has a high ground clearance, under crosswind conditions the aerodynamic drag of the truck will increase due to a crossflow under the truck body. For some trucks without aerodynamic refinement, the drag due to the underbody flow could amount tc about 15% of the overall vehicle drag [1].

Like gap seals, skirts can effectively prevent air flowing across the under body of a truck. Fig. 2.14 shows a truck with side skirts. The decrease in drag due to mounting skirts is less than 8% within yaw angles of 15^0, and the reduction is decreased as the yaw angle varies from 5^0 to 15^0 for a vehicle with trailer skirts [1, 3, 20]. Besides reducing the drag, another advantage of fitting side skirts is that splash and spray can be impeded when a truck is running on a wet road [6].

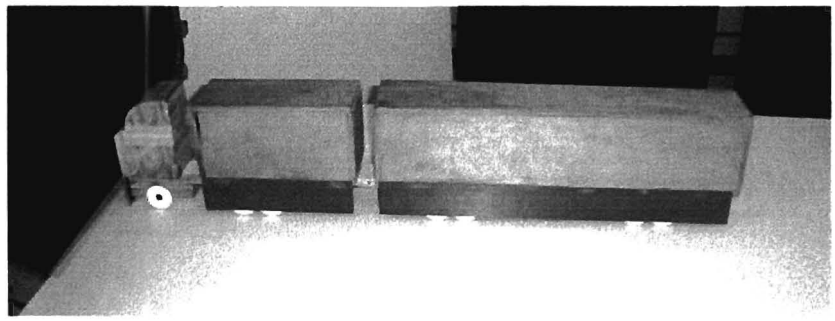

Fig. 2.14: A truck with skirts

- **Trailer rear face fairings**

Rear face fairings are used to increase the pressure on the rear face of trailers. Guide vanes, cavities and splitters shown in Fig. 2.15 are typical of these devices [5].

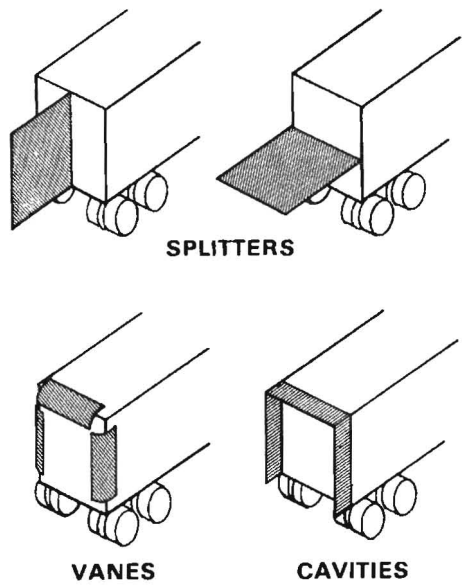

Fig. 2.15: Some rear face fairings

It has been concluded in [3, 21, 22] that fitting guide vanes on the rear face of a trailer does not result in a meaningful drag reduction. Although some researchers believe that with guide vanes there would be a recovery of pressure on the rear surface of trailers [5], this has not so far been proved conclusive in all cases.

It has been found that a cavity is an effective device to reduce drag as a rear face fairing. For a truck, at least a 5% drag reduction is achieved by the addition of cavities fitted to the trailer rear face [5]. The work of Fujimoto et al. [21] shows that the drag coefficient of a small van was reduced from 0.56 to 0.51 after cavities were fitted at the rear face.

2.5 WIND TUNNEL EXPERIMENTS

There are two basic experimental methods used in the research of vehicle aerodynamics: wind tunnel and on-road experiments. A good example of on-road experiments is the work of Steers et al. [23]. However, the scope of this thesis is limited to wind tunnel experiments and in the following paragraphs, some key issues, regarding tests in a wind tunnel, are discussed.

- **Model size**

To obtain the correct aerodynamic characteristics of a truck, it is essential that models tested in wind tunnel experiments should have a very high degree of model detail. Although the scale usually ranges from 1:10 to 1:7, the maximum model size is dictated by the test section size of the wind tunnel [1]. SAE J1252 [24] recommends that the model frontal area at zero yaw angle should not exceed 5% of the active test cross sectional area, while the model height should not exceed 30% of the test section height. Also, the projected frontal

width, when yawed to the maximum angle, should not exceed 30% of the tunnel test section width.

- **Reynolds number**

All researchers are in agreement that as high a Reynolds number as possible should be used. SAE J1252 recommends a minimum Reynolds number of 0.7×10^6. But in the work of Saunders et al. [25], a Reynolds number of 0.3×10^6 was used. When considering the test Reynolds number in conjunction with the typical front corner radii of a tractor, the minimum test Reynolds number is suggested to be from 1.0×10^6 to 2.0×10^6 [1]. Olson and Schaub [26] recommend a Reynolds number test range of 2.2×10^6 to 4.4×10^6 since in this range the drag coefficient is independent of Reynolds number.

In general, Reynolds numbers are based on a particular parameter of the model geometry. This parameter could be the width of the model [17], the length of the model [22], or the effective diameter based on the frontal area [5].

- **Road representation**

In wind tunnel experiments, there is a requirement for a good simulation of the road in order to diminish the ground effect. Due to the boundary layer on the wind tunnel floor, the measured drag is usually less than the real drag of a truck model [27]. Three experimental methods have been used to simulate the road and minimise the ground boundary layer effect:

1) using a moving ground belt
2) using suction to remove the boundary layer
3) using a ground board

The simplest and most common way to represent the road is with a ground board. When the displacement thickness of the floor boundary layer is less than 10% of the vehicle's ground clearance, then using this method, the effect of the boundary layer on the aerodynamic drag of models would be negligible [6]. The work of Cooper et al. is an example of using a ground board in wind tunnel experiments [28].

The use of a moving ground plane is considered as an almost perfect way to simulate the road, since the method can achieve the relative motion between the road and vehicle. For this method, an upstream suction slot is usually used to remove the incident boundary layer [29]. An increase in measured drag of between 5% and 8% was obtained by ground plane movement [30].

The third method to remove the boundary layer is to use a suction system with a perforated surface through which the boundary layer is sucked off. The measured drag of a truck model is increased by about 3.8% after removing the boundary layer by a suction system [27].

2.6 NUMERICAL METHODS

There are fewer research papers in the literature directly related to the numerical modelling of trucks, as opposed to cars or sports cars [31]. An example of modelling a truck is found in reference [32], in which a simple model of a scaled tractor-trailer truck was built with about 12,500 cells.

In general, the simulation of flow over a full-scale truck model will require many thousands of cells to achieve a fine resolution of the flow perturbation caused by fitting aerodynamic drag reduction devices.

CHAPTER 3 - WIND TUNNEL TESTS

With a 1/20 scale double trailer truck model, a series of tests in a low-speed wind tunnel were performed. Initially, some of the wind tunnel tests were carried out to investigate the airflow over the original truck model with no add-on drag reduction devices. Secondly, the add-on devices in various combinations were mounted on the model, and tests conducted to predict the effectiveness of these devices on drag reduction. During the tests the total drag forces were measured for the original tractor-trailer truck model on its own, then with the different add-on devices fitted. In addition, pressure distributions on the top, front and rear surfaces of the trailers were also measured. Flow visualisation studies with cotton tufts were included in the tests.

3.1 EXPERIMENTAL APPARATUS

WIND TUNNEL – The aerodynamic test facility is a re-circulation wind tunnel with an open jet test section, which is situated in the Duncan Macmillan Laboratory of the Department of Mechanical Engineering. The size of the open jet with an octagonal shape is 0.87 m wide by 0.583 m high while the length of the test section is 1.6 m. The area ratio between the settling chamber and test section was 10:1. The velocity variation across the test section was 1% and the turbulence intensity was 0.4%. The maximum air velocity attainable in the test section was 36 m/s (130 km/h). The variation in velocity along the 1.6 m test section was 2.6%, which was small enough to be considered negligible.

While testing, a wooden ground board spanning the testing section was used to simulate the road at the same height as the tunnel floor. Drag forces in the direction of the wind tunnel free stream velocity were measured on a three component wind tunnel balance to an accuracy of 0.02 N.

TRUCK MODEL – On the basis of a South African Breweries (S.A.B.) double trailer Gull Wing truck, a 1/20 scale model with fixed wheels was built with chipboard. For the sake of simplification of analysis, items such as lamps, turning indicators, windows and mirrors as well as underbody structural details were neglected during the construction of the model. The overall size of the model was 1100 x 130 x 215 mm, with the tractor having a width of 110 mm and height of 160 mm. The gap between the back of the cab and the first trailer was 45 mm while the gap between the two trailers was 33 mm. Fig. 3.1 shows the profile of the truck model. The blockage ratio was 5.5%, which is defined as the ratio of the cross-sectional area of the vehicle to the cross-sectional area of the wind tunnel jet [33].

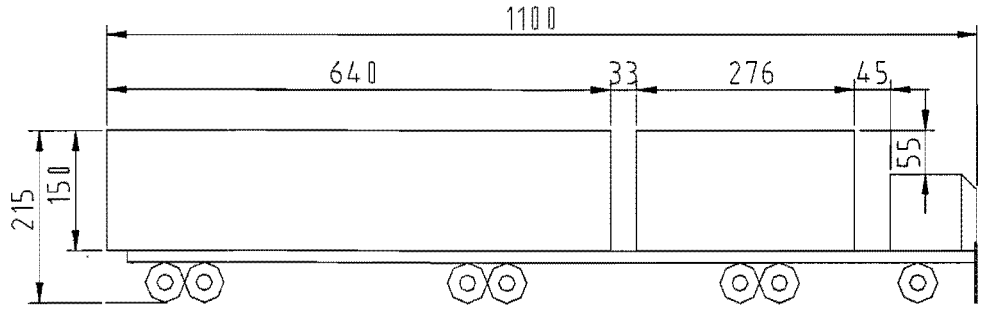

Fig. 3.1: Dimensions of the original truck model

Surface pressure tappings were distributed on the front, rear and top surfaces of the two trailers. At the condition of zero-yaw angle, the airflow over the truck is assumed to be symmetrical about its vertical center plane, thus pressure symmetrical tappings were placed only on one half of the surface. The positions of the tappings on the front trailer surfaces are shown in Fig. 3.2. The tappings take the form of 1.5 mm diameter copper tubes flush with each surface. The tubes were brought through the inside of the model and connected via plastic tubing to a digital manometer, as shown in Fig. 3.3. The total number of pressure tappings on one surface is 15, with the exception of the top surface of the rear trailer which has 36.

ADD-ON DEVICES - There are five basic sources which contribute to the aerodynamic drag on a commercial vehicle: front-surface pressure, rear-surface pressure, airflow across tractor-trailer gap, underbody airflow and skin friction. Usually, the first four sources produce the major portion of the total aerodynamic drag of the truck. For example, for a mid 1970's tractor-trailer truck, up to 95 percent of the total aerodynamic drag is developed by these four sources [1].

In this project, numerous add-on drag reduction devices in various forms were designed and constructed for the model. They were fitted on the original truck model in various combinations and include a cab deflector, gap seals, side skirts and rear-base fairings. Fig. 3.4 shows the profile of a model with some add-on drag reduction devices. Each add-on device is easily attached to the original truck model, and its weight is kept as light as possible by the selection of suitable construction material. The surfaces of the models with and without add-on devices are kept smooth.

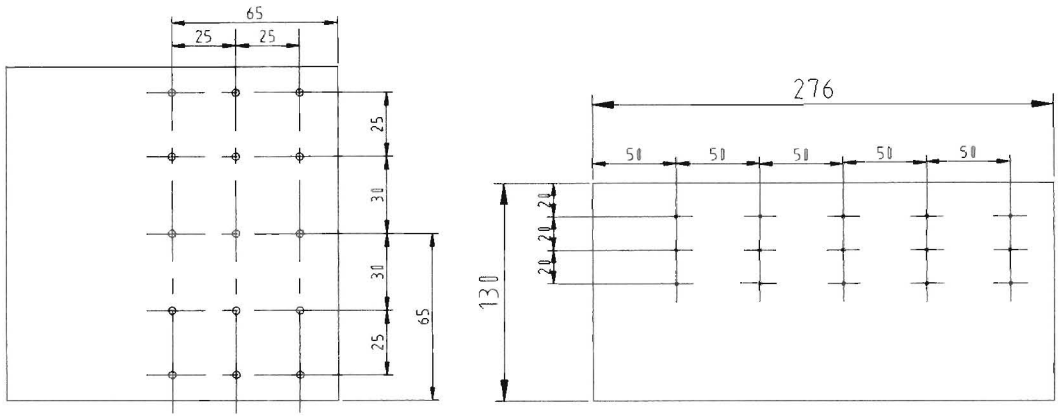

a: Front surface b: Top surface

Fig. 3.2: Tappings distributed on surfaces of the front trailer

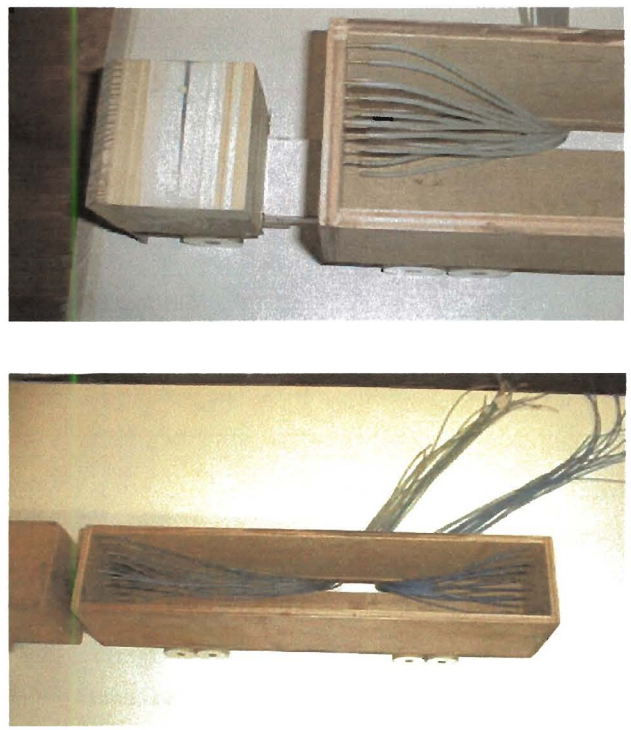

Fig. 3.3: Pressure tapping tubes leading from the trailer surfaces

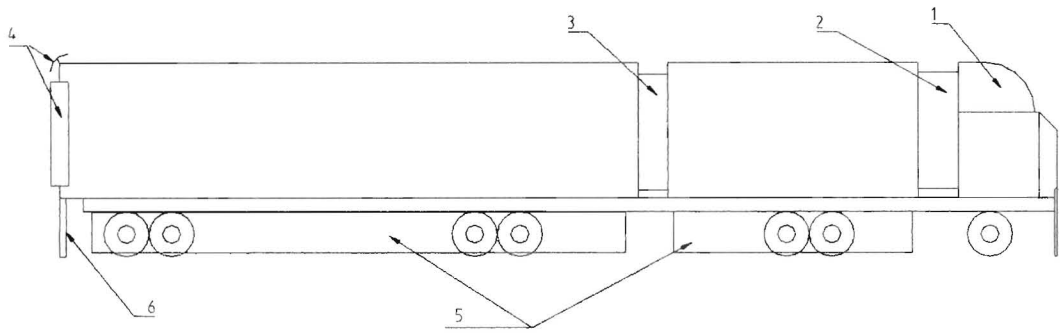

1. Cab deflector
2. The first gap seal
3. The second gap seal
4. Guide vanes
5. Side skirt
6. The rear fender

Fig. 3.4: The truck model with add-on devices

- **Cab deflector and side skirts**

A wooden cab deflector (1) in Fig. 3.4 was used to reduce the pressure on the front vertical face of the front trailer. The cab deflector is the same width as the cab roof, and has a height equal to that of the trailers. Its shape and dimensions are shown in Fig. 3.5. Since the gap between the back of the tractor and the front trailer was comparatively large, there was no attempt to design a container forebody fairing for drag reduction in the tests. Another reason is that with a cab deflector, gap seals can be easily fitted on the model.

Considering the geometric characteristic of the double trailer truck, only the trailers were fitted with side skirts. A distance of 10 mm was left between the side skirts and the ground board. Fig. 3.6 shows a model with the deflector and side skirts.

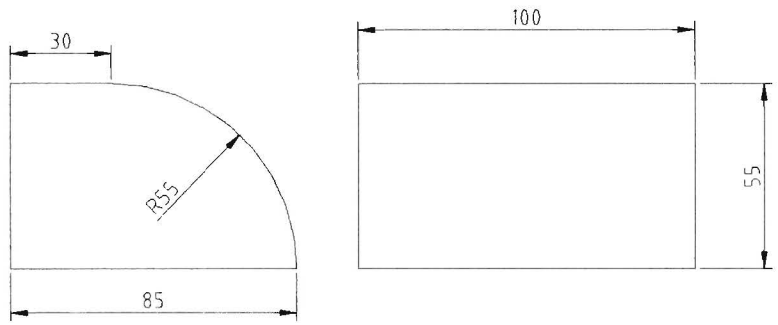

Fig. 3.5: Dimensions of the cab roof deflector

Fig. 3.6: The model with the cab deflector and skirts

- **Gap seals**

In order to investigate the influence of the gaps between the cab and front trailer and the two trailers on the truck drag, two types of gap seals were tested in the experiments: center gap seal and side gap seal. Both gap seals had the same height, which was a little less than that of the trailer box. The center gap seal was placed along the central line of the longitudinal axis of the truck in the gaps between the cab and the trailer, and the two trailers as shown in Fig. 3.7.

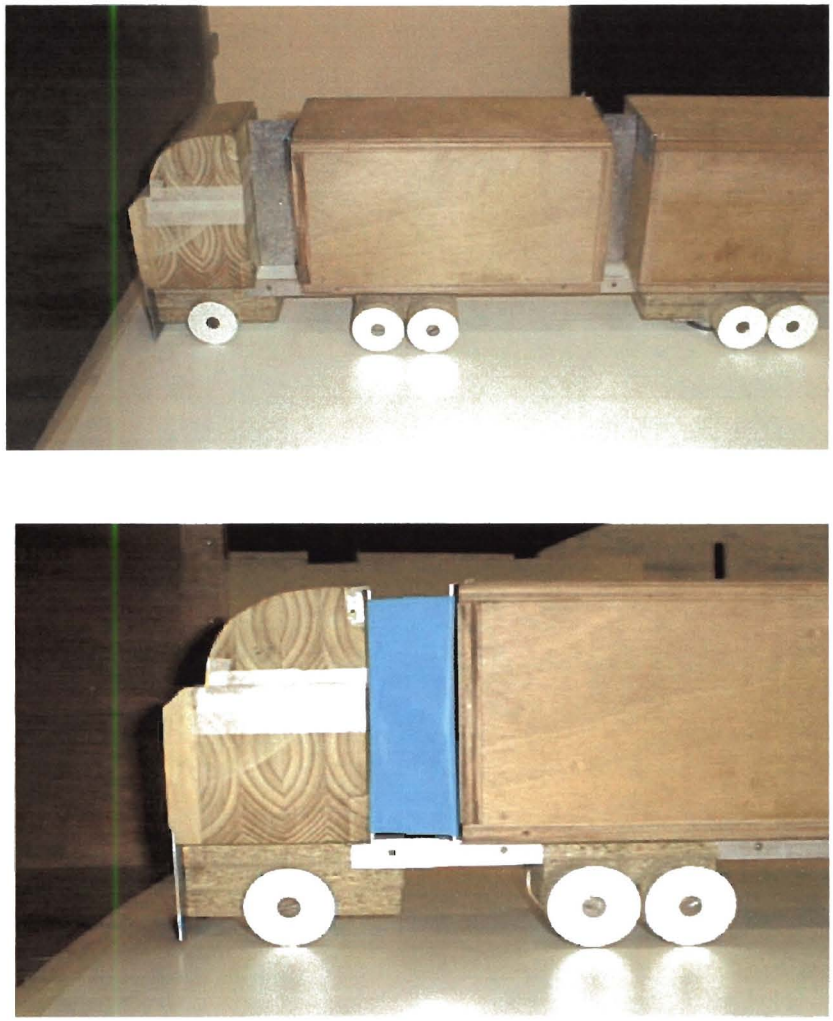

Fig. 3.7: Models with gap seals

Side gap seals were used to prevent transverse airflow through the gaps as shown in Fig. 3.7. Their design is shown in Fig. 3.8. Considering the truck maneuverability, the cloth should in practice be made of a flexible material. However, in this project a plastic cloth was selected. Since the length of the gap between the two trailers is so small, it was directly sealed using tapes from two sides as the side gap seal.

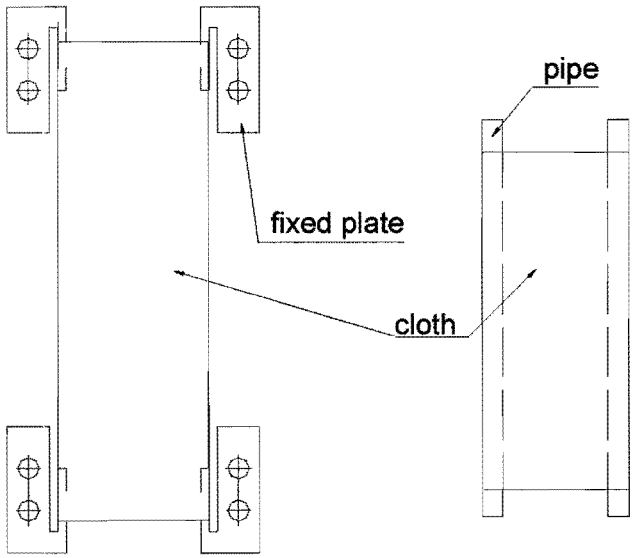

Fig. 3.8: Structure of a side gap seal

- **Rear face fairings**

Rear cavities, edge fairings and guide vanes are selected as rear face fairings. The purpose of using these add-on devices is to investigate their effect on the pressure on the rear vertical face of the rear trailer. The cavity depth and radius of the guide vanes and edge fairings are all 8 mm, half of the effective diameter of 15.6 mm. The gap between the guide vanes and trailer's surface was 4 mm. The rear face fairings are shown in Fig. 3.9. Although guide vanes were not likely to result in an extra drag reduction [3, 21, 22], their effect on the pressure acting on the rear face of the rear trailer was investigated. To compare the effectiveness of the rear face fairings, a rear fender was also tested as an add-on device.

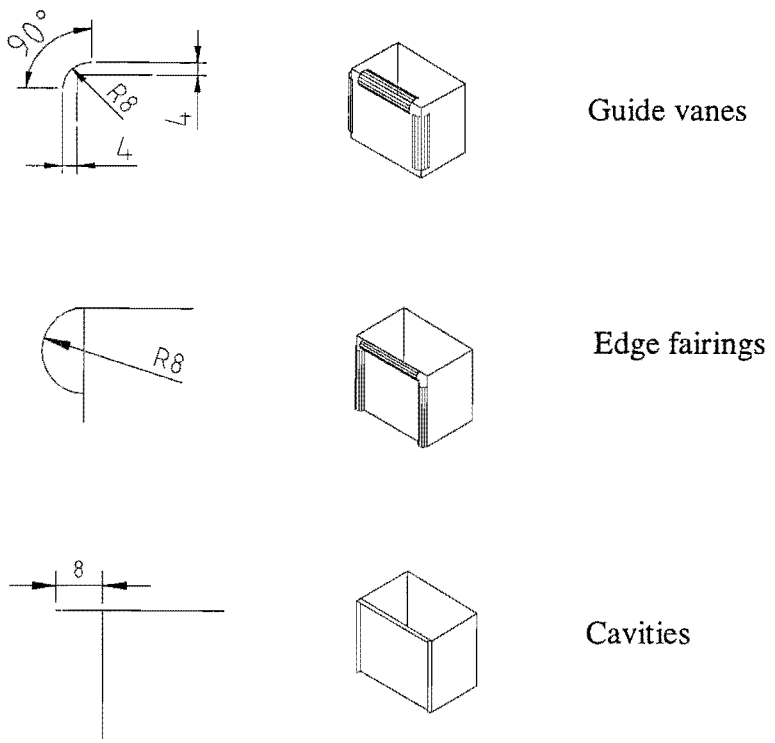

Fig. 3.9. Base-mounted devices

3.2 MODEL MOUNTING

At the open jet test section, the truck model was mounted above the ground board on the wind tunnel balance by using a sting located in the model's underside at the position of 560 mm from the front edge of the model. A gap of 2 mm was left between the wheels and the ground board in order to exclude friction forces. Fig. 3.10 shows the set up of the truck model in the wind tunnel.

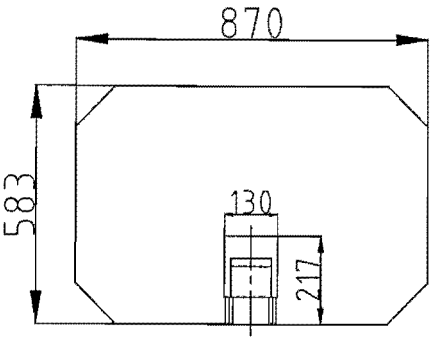

a: Front view

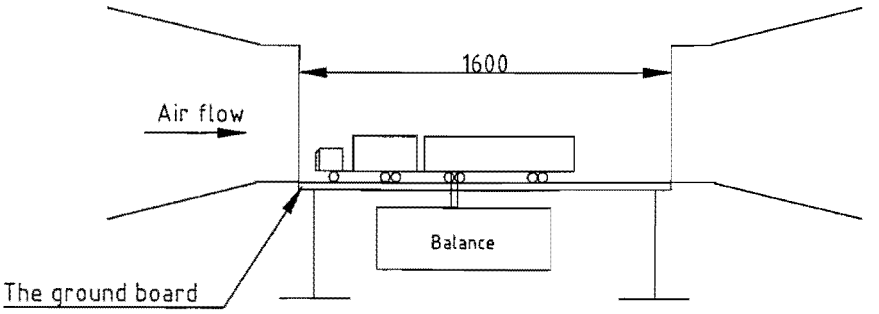

b: Side view

Fig. 3.10: Wind tunnel test section and model installation

3.3 EXPERIMENTAL PROCEDURE

The drag measurements were conducted initially with the original truck model. Then add-on air deflection devices in various combinations were mounted on the original model and new drag measurements taken.

Drag measurement - The three component balance below the ground board was used to measure the drag forces on the truck models in the direction of the wind tunnel free stream velocity. A digital display enabled the drag in Newtons to be determined. The formula for the conversion is:

$$\text{Drag} = (\text{display reading} - \text{zero display reading}) \times 2 \quad \text{N} \qquad (3.1)$$

Drag tests were carried out at test section wind speeds ranging from 40 to 110 km/h and at yaw angles of 0^0 and 5^0. The corresponding Reynolds numbers ranged from 0.94×10^5 to 2.59×10^5 based on the total width (W = 0.13 m) of the model. In all tests, the drag was first measured with no wind, then a wind speed was set and a new drag measured. The difference in readings gave the measured drag force D_m.

Since all the drag forces were measured in the direction of the wind tunnel free stream velocity, they were converted to the body axis referred to the model. Before converting, a truck body axis system must be defined. The systems are defined graphically in Fig. 3.11. A yaw angle β is defined as the angle between the free stream velocity and the longitudinal axis of the model. At zero-yaw, D_m equals the drag D of the model in the truck body system. At a yaw angle, D is calculated from:

$$D = D_m \cos\beta \qquad (3.2)$$

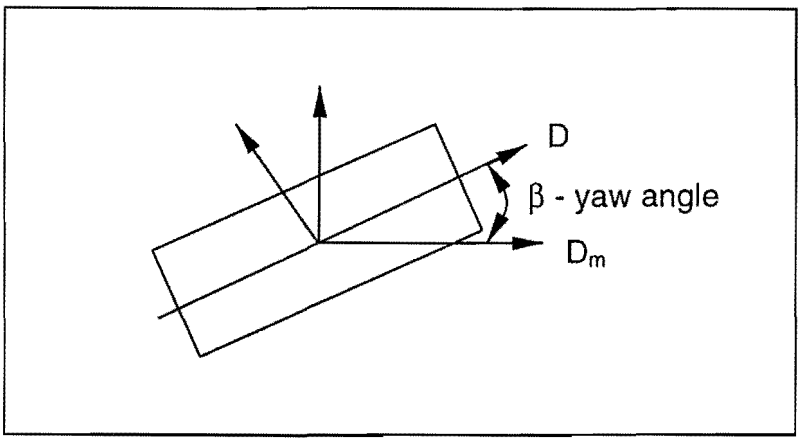

Fig. 3.11: The yaw angle and axis systems

The results are presented in terms of drag coefficient, which were calculated from the following equations:

$$C_D = \frac{D}{\frac{1}{2}\rho V^2 A} \qquad (3.3)$$

where D is the drag force, V the free stream velocity and ρ the density of air. The reference area A was 0.02795 m^2 (the total height times the total width, 0.13 x 0.215 mm).

While measuring drag forces, the plastic tubes for pressure measurement were housed inside the model body and, the bottom floors of the trailers were sealed with steel plates. No blockage correction was made to the results because the blockage correction in an open jet wind tunnel is usually very small and may be considered negligible [34].

Pressure measurement - A digital manometer with a maximum range of 1000 Pa was used for measuring the pressures on the surfaces of the trailers. The positive pressure tapping of the manometer was connected to the tubes on the surfaces of the trailers, while the negative one was open to atmosphere, thus the readings taken from the digital manometer were the pressures relative to the atmospheric pressure.

Tests for measuring the pressure distribution were conducted at a wind speed of 80 km/h and zero-yaw, equivalent to a Reynolds number of 1.6×10^5 based on the total width of the truck. Following the original truck model tests, models with one add-on drag reduction device were selected and the pressure distributions on the surfaces of the two trailers were measured.

Based on the pressure data collected from the wind tunnel tests, the corresponding pressure coefficients were obtained from the equation (3.4):

$$C_p = \frac{P - P_\infty}{\frac{1}{2}\rho V^2} \qquad (3.4)$$

where P is the static pressure at a tapping and P_∞ the static atmosphere pressure.

CHAPTER 4 - DISCUSSION OF EXPERIMENTAL RESULTS

The experimental results are discussed in this chapter. It begins with the discussion of the drag forces, followed by that of the pressure distributions on the various faces of the trailers. All the drag and pressure coefficients presented in the tables of this section are at a Reynolds number of 1.6×10^5 based on the total width of the model.

4.1 DRAG FORCES

Drag coefficients for the models with various combinations of cab deflector (CD), side skirts (SS), center and side gap seals (CGS, SGS) at yaw angles of 0^0 and 5^0 are listed respectively in Table 1 and Table 2. The corresponding drag coefficient curves versus Reynolds numbers are shown separately in Fig. 4.1 and Fig. 4.2.

- **At a yaw angle of 0^0**

Under the condition of zero-yaw, the drag coefficient of the original truck on its own is 0.9283. From Table 1, it is seen that the addition of either center or side gap seals did not decrease the drag, which is consistent with the conclusion of Marks and Buckley [17]. However, a drag reduction was obtained by adding the side skirts. The reductions in drag coefficient due to the side skirts are less than 4%, whether they were used on their own or in combination with other add-on devices (Table 1).

The greatest reduction of 30% in C_D was achieved with the combination of cab deflector, side skirts and side gap seals. Compared to the center gap seal, this could suggest that side gap seals have an influence on the airflow under the

truck body. Actually, the amount of air flowing down the gap can be decreased by side gap seals.

Table 1 Drag coefficients of models at $\beta = 0^0$, V = 22 m/s

Model	Original Truck	Cab Deflector	Side Skirts	CD + CGS	CD + SGS	CD + SS	CD+SS +CGS	CD+SS + SGS
C_D	0.9283	0.6806	0.8899	0.6878	0.6782	0.6686	0.6686	0.6494
Reduction		-26.7%	-4.1%	-25.9%	-26.9%	-28.0%	-28.0%	-30.0%

Table 2 Drag coefficients of models at $\beta = 5^0$, V = 22 m/s

Model	Original Truck	Cab Deflector	Side Skirts	CD + CGS	CD + SGS	CD + SS	CD+SS CGS	CD+SS SGS
C_D	1.088	0.997	1.023	0.879	0.877	0.961	0.822	0.771
Reduction		-8.4%	-6.0%	-19.2%	-19.4%	-11.7%	-24.4%	-29.1%

The cab deflector was the most effective device, giving a drag reduction of 26% of that of the original truck. Fig. 4.3 shows that the flow separation on the top forward edge of the front trailer is removed by the addition of the cab deflector.

From Fig. 4.1, it is observed that for the original truck model and the models with various combinations of the cab deflector, side skirts and gap seals, their drag coefficients decrease as the Reynolds number increases from 0.94×10^5 to 1.41×10^5. It is then followed by an increase of the drag coefficients while the Reynolds number further increases to 1.65×10^5. The drag coefficients were invariant for Reynolds numbers above 1.65×10^5.

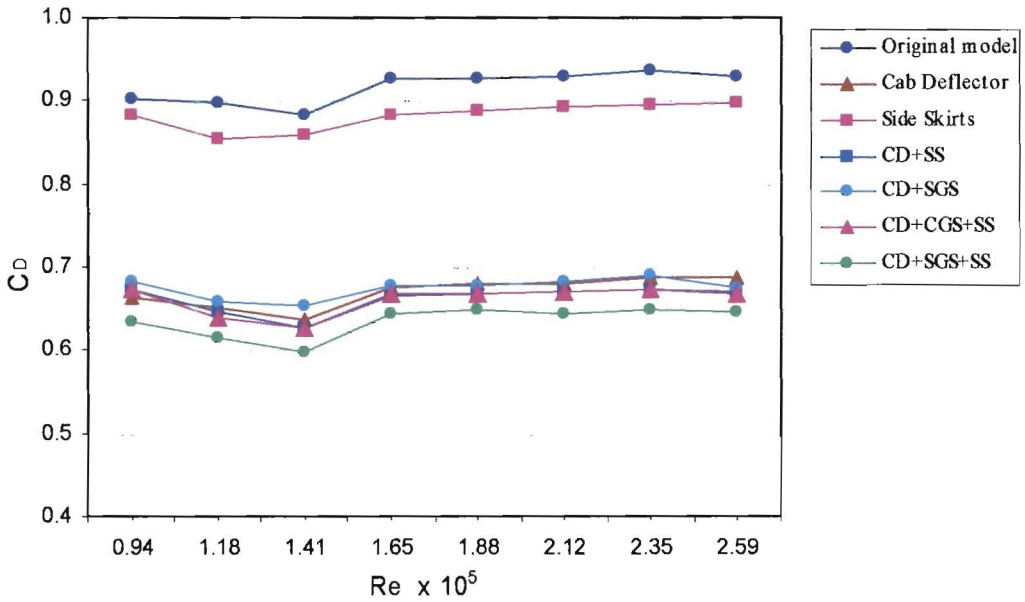

Fig.4.1: Drag coefficient versus Reynolds number for models at $\beta=0^0$

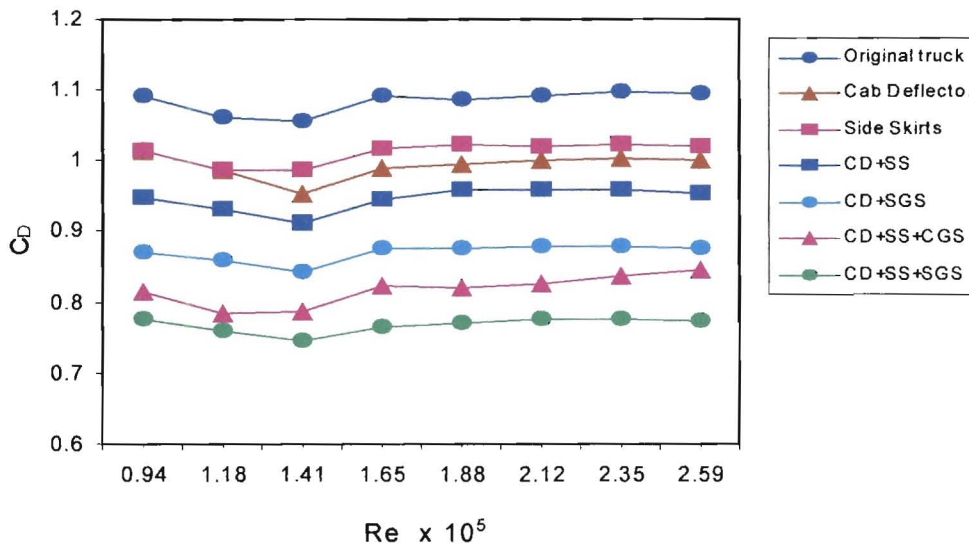

Fig.4.2: Drag coefficient versus Reynolds number for models at $\beta=5^0$

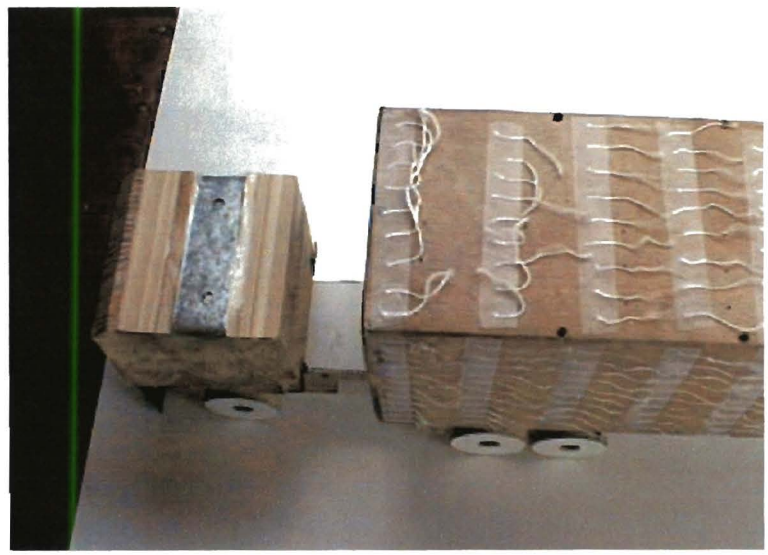

a: flow separation on the top edge

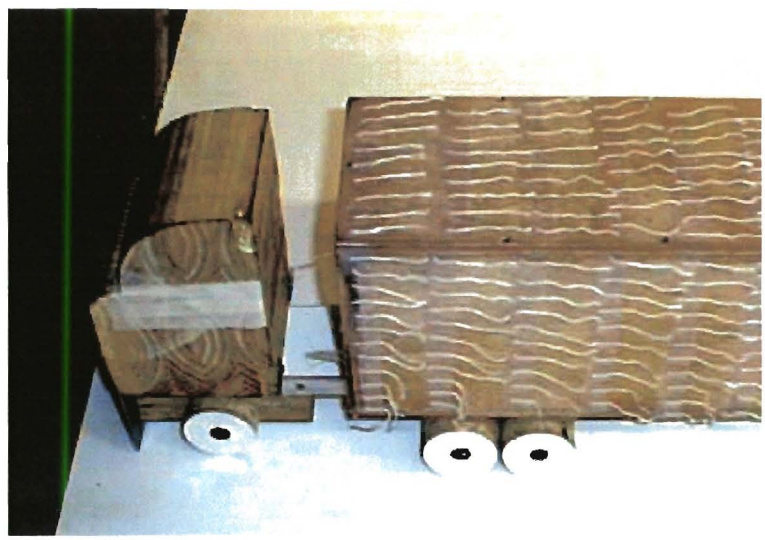

b: no separation at the top edge

Fig. 4.3: Flow separation before and after adding the cab deflector

Curves of the percentage reduction in drag for models with rear face fairings are shown in Fig. 4.4. For Reynolds numbers ranging from 0.94 x 10^5 to 2.59 x 10^5, either guide vanes or rear fender produce a drag increase of 5% to 7%. Considering their effect on drag reduction, guide vanes seem to act as a rear fender. It is interesting to note that as the Reynolds number increases the drag increase is reduced for the model with guide vanes. This indicates that at higher Reynolds numbers, guide vanes might produce a pressure recovery on the rear face of the rear trailer.

With either rear cavities or edge fairings, the drag reductions are less than 3% at low Reynolds numbers. A sudden drop in drag occurred at higher Reynolds numbers, which led to the largest drag reduction of about 6%. This indicates that rear cavities and edge fairings are more effective on drag reduction at higher Reynolds numbers (i.e. high truck speeds).

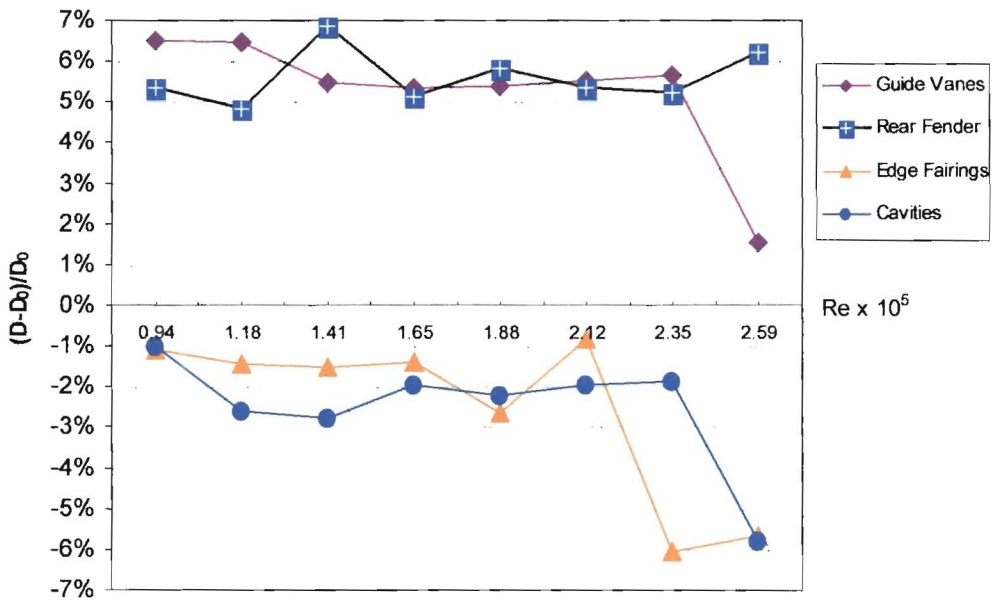

Fig. 4.4: Drag reduction due to rear face fairings

D: drag for models with drag reduction devices

D_0: drag for the original model

- **At a yaw angle of 5^0**

At 5^0 yaw, the drag of the original model is considerably increased (Fig. 4.5) and, a flow separation on the leeward side of the front trailer was clearly observed (Fig. 4.6). The drag coefficient (Table 2) is increased by 17.2 percent, from 0.9283 to 1.088, in comparison with the case of zero-yaw angle. Therefore, the drag caused by the airflow across the gap and the underbody becomes a substantial part of the aerodynamic drag on a tractor-trailer truck when the truck is yawed to the wind.

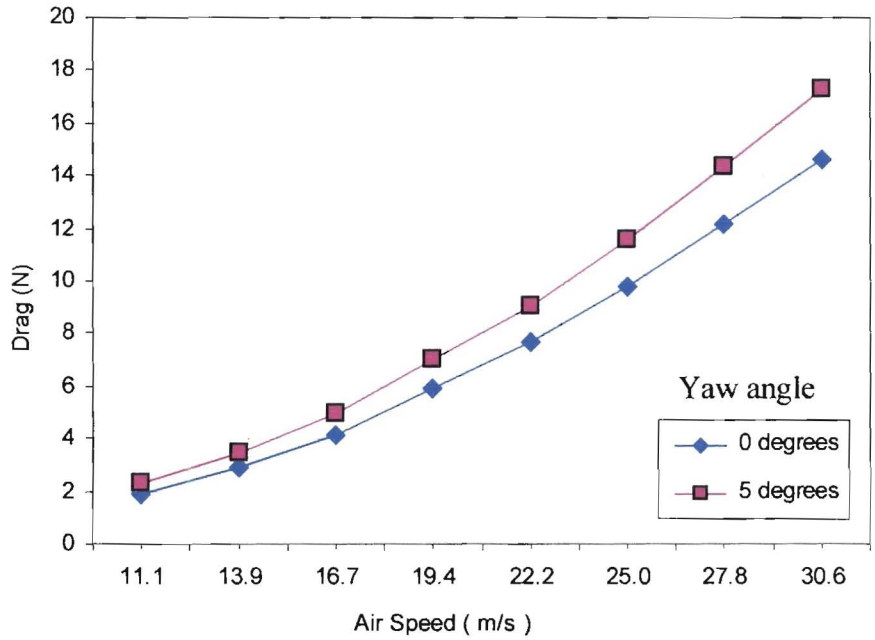

Fig. 4.5: Drag curves for the original truck model

At $\beta = 5^0$, only 8.4% of drag reduction was obtained by adding the cab deflector, which is much less than the 26% drag reduction at zero-yaw angle. This is similar to the conclusion of Marks et al. [7], that, the effectiveness of a cab deflector on drag reduction can be considerably decreased as the yaw angle increases up to 10^0. A cab deflector is not effective in reducing the drag caused by the airflow between the cab rear and trailer forebody.

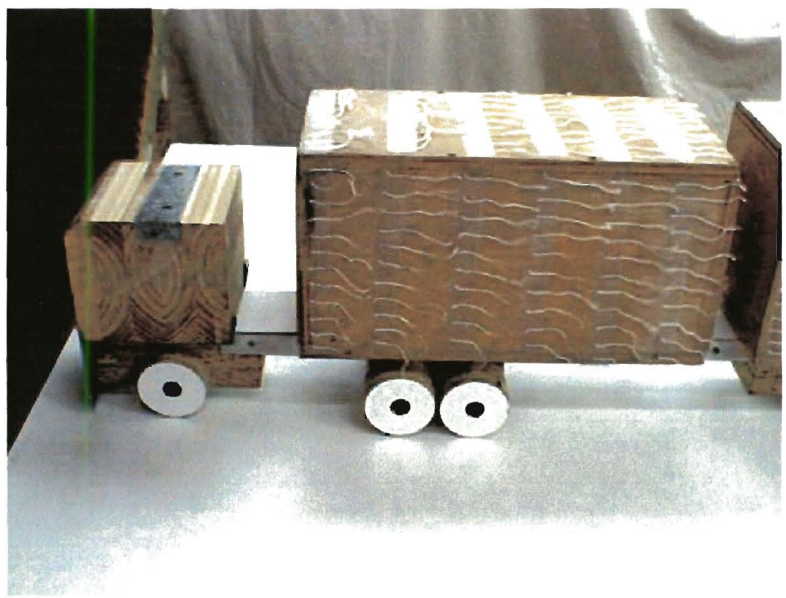

a: the original truck at $\beta=0^0$

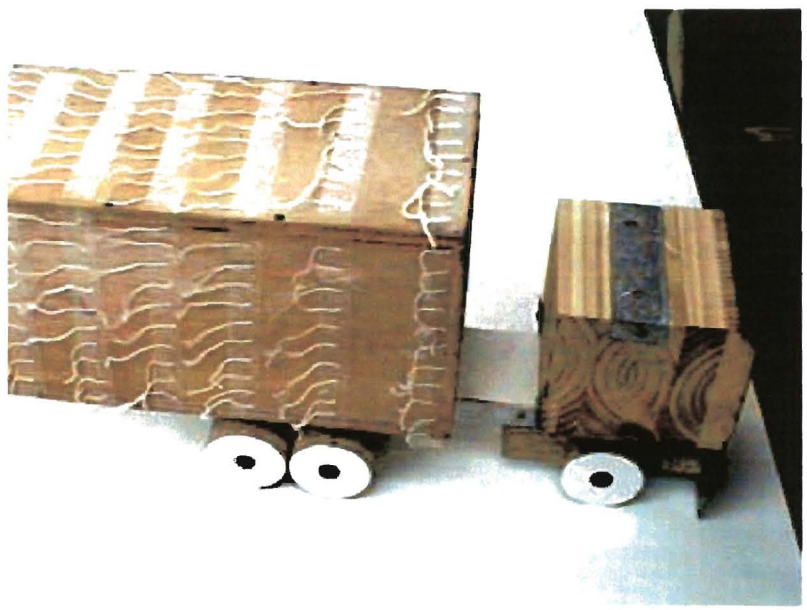

b: the original truck at $\beta=5^0$

Fig. 4.6: Flow separation for the original truck

The airflow across the gap is vitally important when considering the aerodynamics of a tractor-trailer truck under crosswind conditions. As mentioned in section 2.4, gap seals are more effective in drag reduction at a yaw angle. With the cab deflector in position, 10.8% and 11% of extra reduction in drag coefficient were obtained respectively by adding center and side gap seals (Table 2).

From Fig. 4.7, it is clearly observed that the air flow over the rear trailer causes little separation at a yaw angle of 5^0. It is also seen that the addition of gap seals did not improve the flow separation on the leeward side.

It is interesting to note that the addition of center gap seals and side gap seals to the 5^0 yawed model which was already fitted with the cab deflector and side skirts, further reduced C_D by 5% and 10% respectively (Table 2). The drag coefficient with side gap seals is about 5% more than that with a center gap seal. Compared with the cases without side skirts (Table 2), this further confirms that side gap seals have a profound influence on the flow under the truck body, especially under crosswind conditions. A center gap seal has no effect on the under-body flow of a truck.

At yaw, the addition of side skirts gave a 6.6% reduction in drag coefficient, and yielded a drag reduction of 11.7% in combination with the cab deflector. Compared with the 4.1% reduction at zero yaw, only 2.5% extra reduction was obtained by adding side skirts at a yaw angle of 5^0. This shows the limitation of reducing drag by adding side skirts.

Drag coefficient curves in Fig. 4.2 shows similar trends to those in Fig. 4.1, which suggests that over the given range of Reynolds number, the drag characteristic of the truck does not vary with yaw angle.

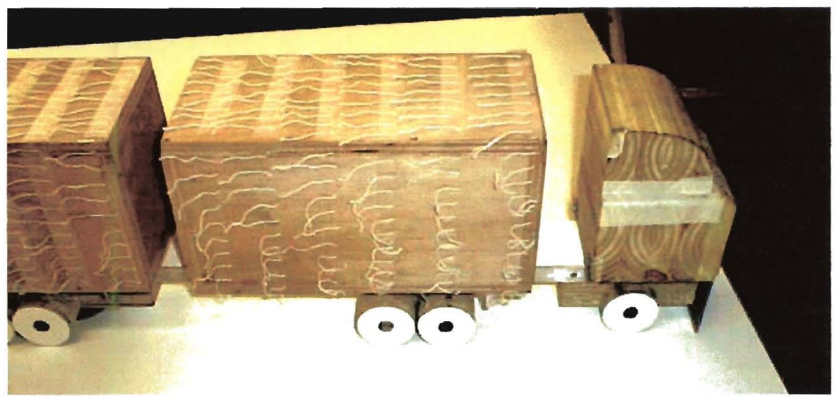

a: cab deflector only

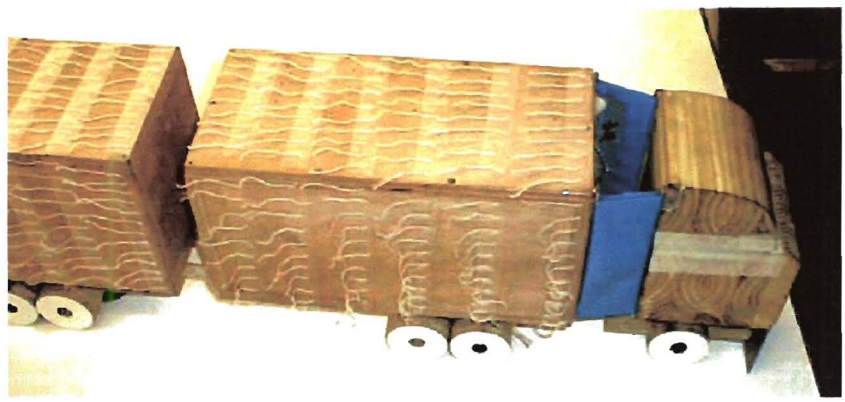

b: cab deflector with side gap seals

c: cab deflector with center gap seal

Fig. 4.7: Flow separation for models with or without gap seals

4.2 PRESSURE DISTRIBUTIONS

Pressure distributions on the trailers' surfaces are presented in Figs. 4.8 to 4.12, while the mean pressure coefficients on those surfaces are listed in Tables 3 – 6.

For the original model, the pressure on the front face of the front trailer is mainly positive, that is greater than the static atmospheric pressure P_∞. After adding the cab deflector, negative pressures were obtained, resulting in a 260% reduction in the mean pressure coefficient. Adding center or side gap seals did not further reduce the mean pressure coefficient, and explains why an increased drag reduction is not obtained at zero-yaw.

The pressure coefficient on the front face of the rear trailer is generally negative (Fig. 4.9a). With side gap seals and cab deflector, it becomes even more negative (Fig. 4.9d), but with the cab deflector alone it becomes positive with respect to P_∞ (Fig. 4.9b). A center gap seal with the cab deflector also produces an increase in pressure with respect to the static atmospheric pressure (Fig. 4.9c). However, these changes hardly affect the value of C_D with the cab deflector alone (Table 1).

From Table 6 and Fig. 4.10, it is clear that both the guide vanes and the rear fender decrease the pressure on the back surface of the rear trailer, and accounts for why the guide vanes did not reduce the drag on a truck. With rear cavities, a 13.5% increase in mean pressure coefficient was achieved, thus indicating their effectiveness in increasing the pressure on the back face. Side skirts also produce an increase in pressure on the rear trailer back surface, resulting in a small reduction in drag.

The pressure distributions on the rear face for the models with cavities and edge fairings are similar to that of the original model, except for the different pressure values for each case (Fig. 4.10). In fact, the addition of cavities and

edge fairings did not change the projected cross sectional area of the rear face of the rear trailer, but the rear trailer box becomes slightly longer.

On the top surface of the front trailer of the original model, lower pressures were measured near the front forward edge where a flow separation occurs. By the addition of the cab deflector, the pressure on the top surface was considerably increased, being close to P_∞. For the rear trailer, the pressure on the front part of the top surface was close to the free stream pressure, while the pressure on the back part was a little lower than P_∞ (Fig. 4.12). Although there was a small change in pressure coefficient on the top surface of the rear trailer due to adding the cab deflector, it might be considered that the pressure on this surface is constant since the absolute value of the change was very small.

The whole numbers in Fig. 4.8 – Fig. 4.12 refer to the positions of the pressure tappings distributed on the surfaces of the trailers, shown as follows:

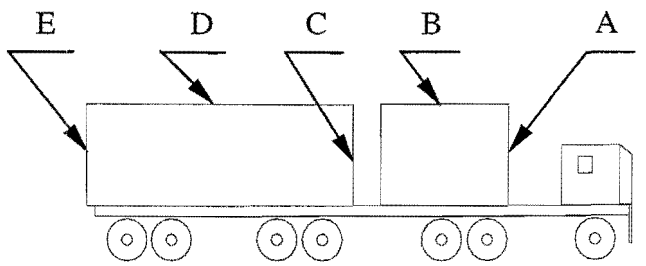

Surface A, C, E

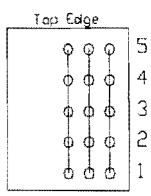

Surface B

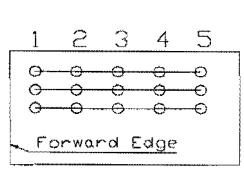

Surface D

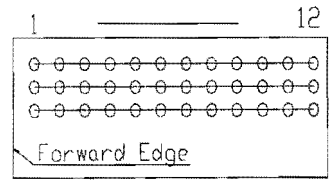

Table 3: Pressure coefficients on the front face of the front trailer

	Original Model	Cab Deflector	Cab Deflector Center Gap Seals	Cab Deflector Side Gap Seals
Mean C_P	0.1800	-0.2919	-0.2891	-0.2891
C_P-C_{P0}		-0.4719	-0.4691	-0.4691
$(C_P-C_{P0})/\|C_{P0}\|$		-262.2%	-260.7%	-260.7%

Table 4: Pressure coefficients on the front face of the rear trailer

	Original Model	Cab Deflector	Cab Deflector Center Gap Seals	Cab Deflector Side Gap Seals
Mean C_P	-0.0323	0.0172	-0.0130	-0.0814
C_P-C_{P0}		0.0495	0.0193	-0.0492
$(C_P-C_{P0})/\|C_{P0}\|$		153.2%	59.7%	-152.3%

Table 5: Pressure coefficients on top surfaces of the trailers

	Original Model		Cab Deflector	
	Front Trailer	Rear Trailer	Front Trailer	Rear Trailer
Mean C_P	-0.1525	-0.0069	-0.0312	-0.0090
C_P-C_{P0}			0.1214	-0.0021
$(C_P-C_{P0})/\|C_{P0}\|$			79.6%	-31.0%

Table 6: Pressure coefficients on the rear face of the rear trailer

	Original Model	Side Skirts	Guide Vanes	Rear Cavities	Edge Fairings	Rear Fender
Mean C_P	-0.0843	-0.0792	-0.1259	-0.0729	-0.0791	-0.1162
C_P-C_{P0}		0.0051	-0.0416	0.0114	0.0052	-0.0319
$(C_P-C_{P0})/\|C_{P0}\|$		6.1%	-49.4%	13.5%	6.1%	-37.9%

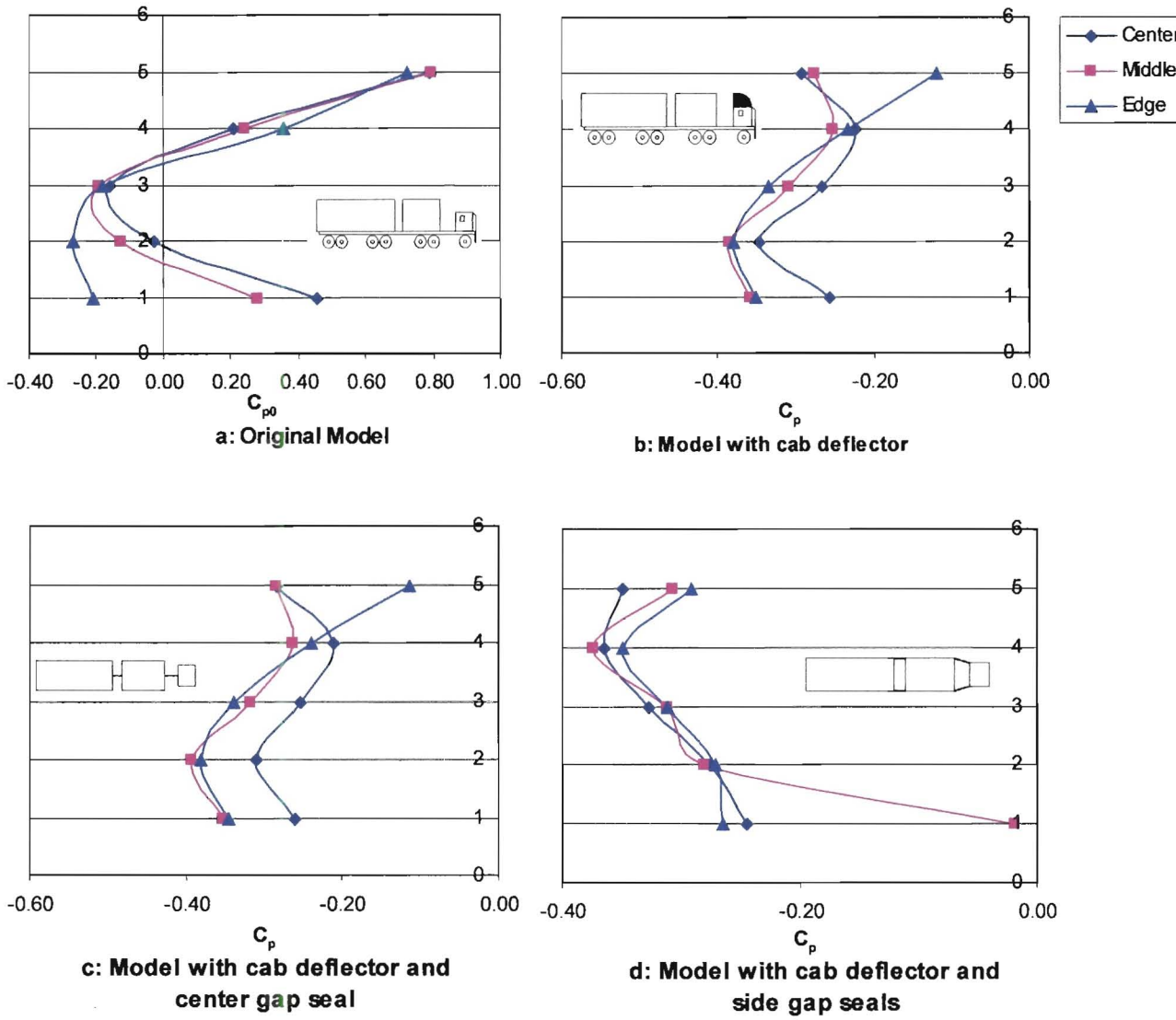

Fig. 4.8: Pressure distributions on the front surface of the front trailer

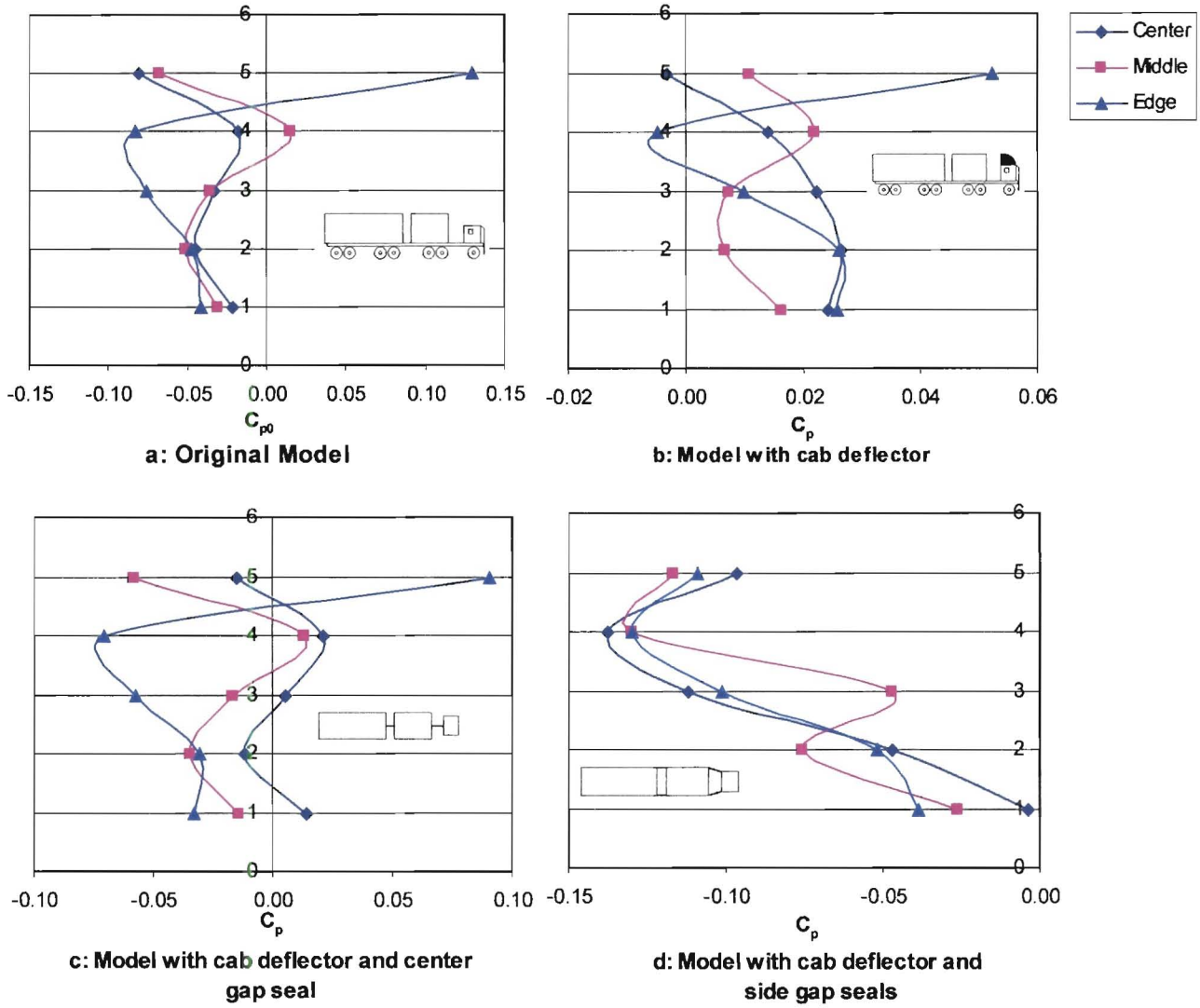

Fig. 4.9: Pressure distributions on the front surface of the rear trailer

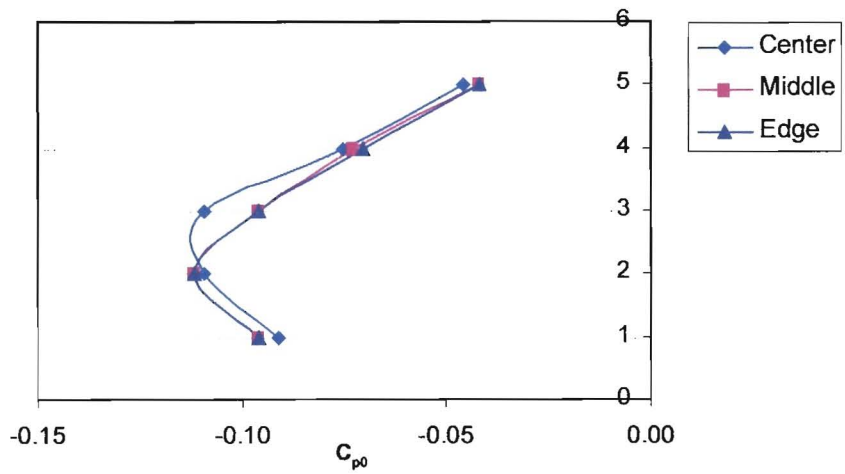

a: Original truck model

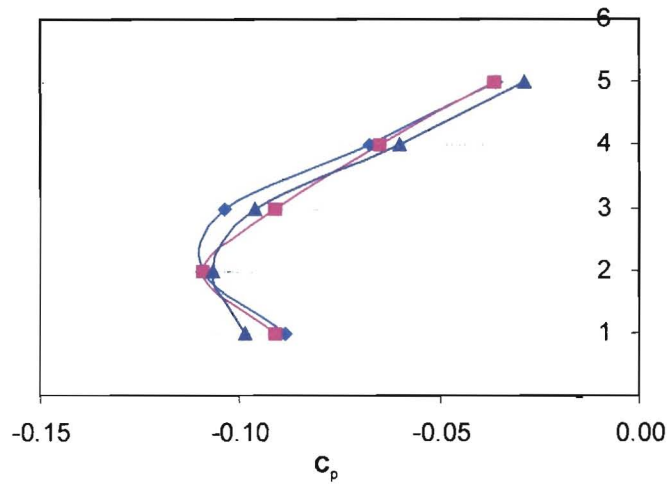

b: Model with Edge Fairings

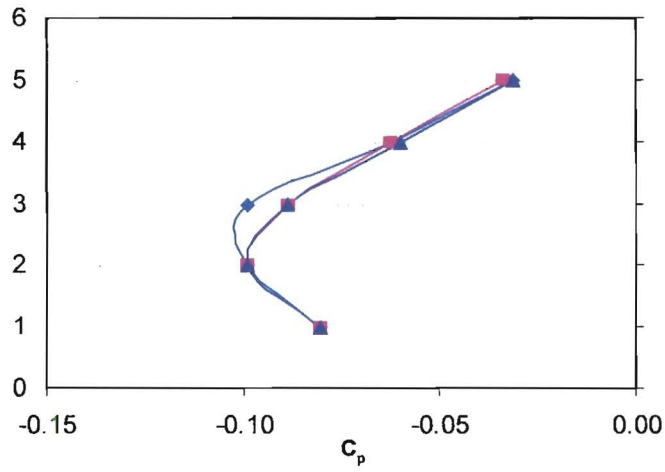

c: Model with Cavities

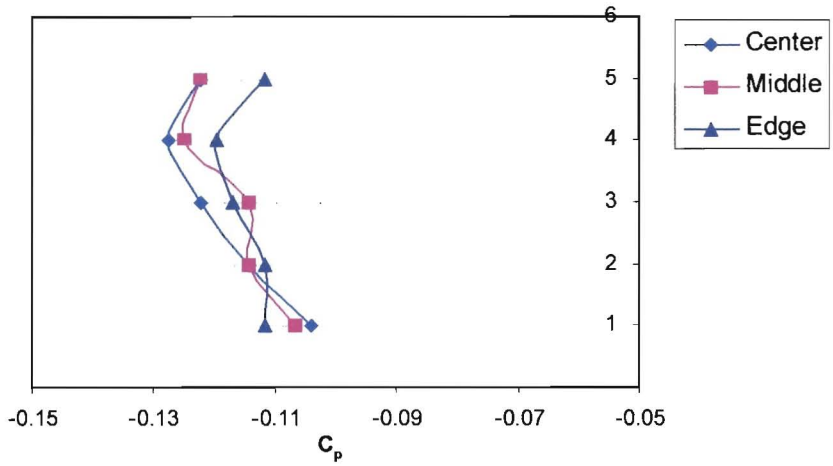

d: Model with Rear Fender

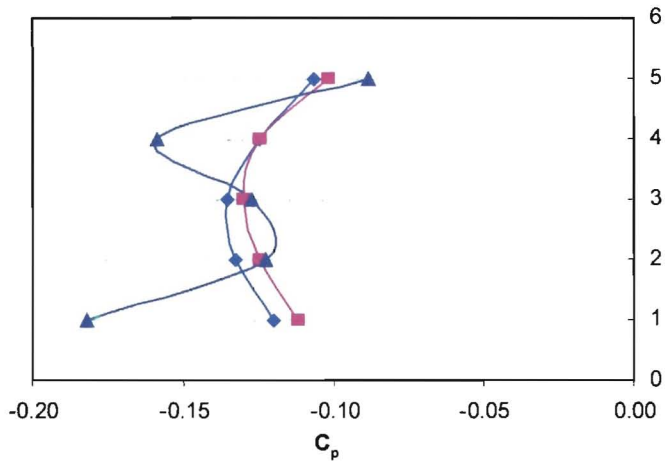

e: Model with Guide Vanes

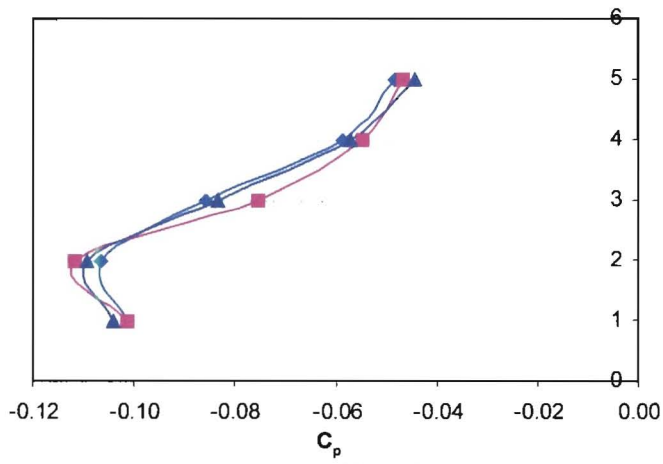

f: Model with Side Skirts

Fig. 4.10: Pressure distributions on the rear surface of the rear trailer

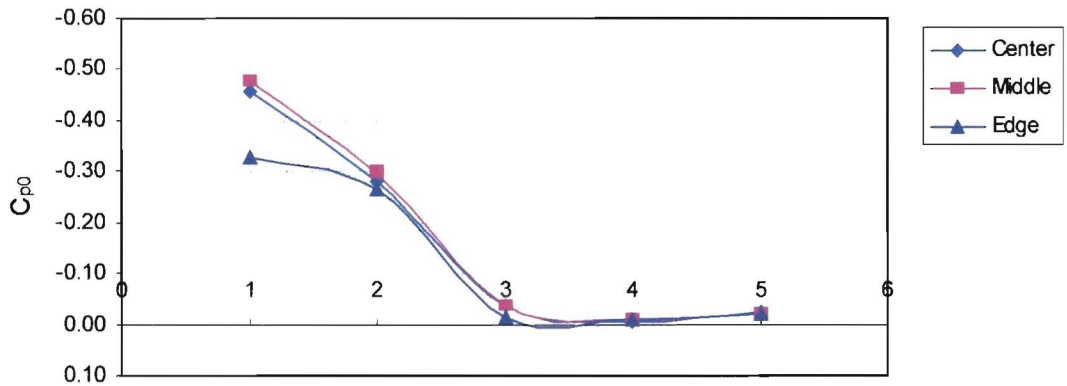

a: Original Model

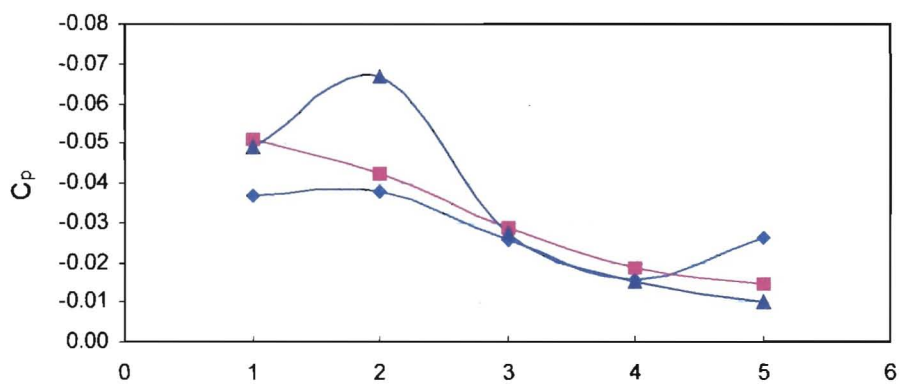

b: Model with Cab deflector

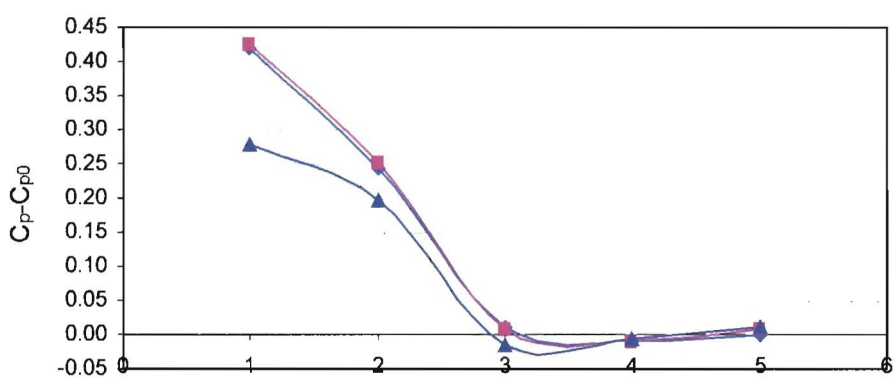

c: Difference in pressure coefficient

Fig. 4.11: Pressure distributions on the top surface of the front trailer

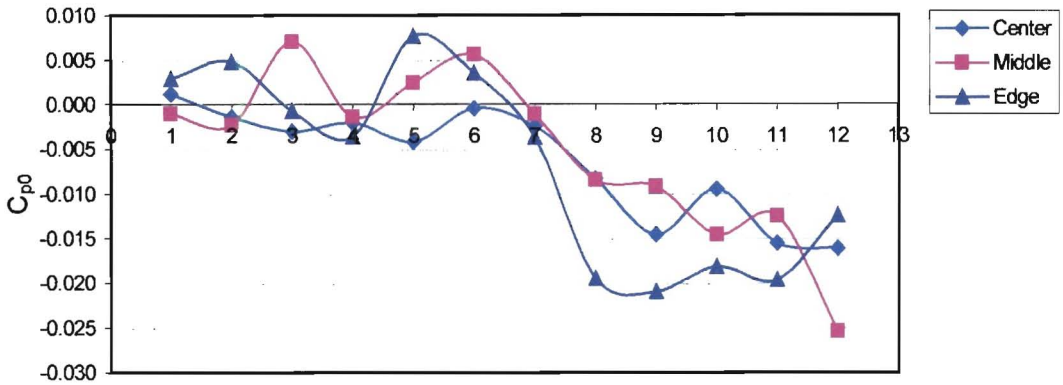

a: Original Model

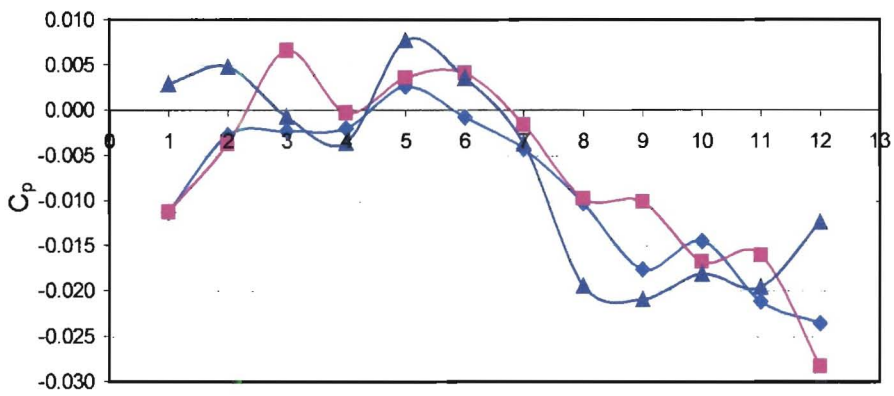

b: Model with Cab deflector

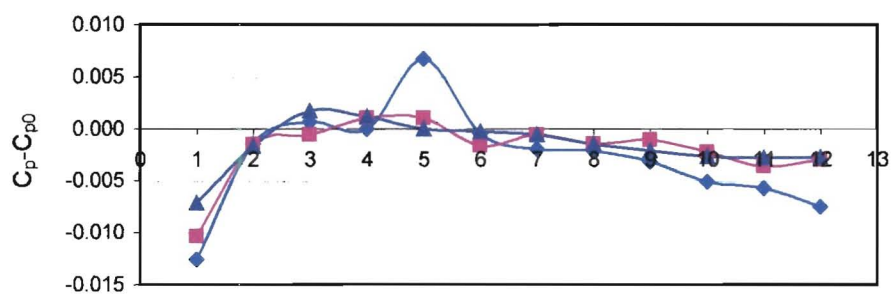

c: Difference in pressure coefficient

Fig. 4.12: Pressure distributions on the top surface of the rear trailer

CHAPTER 5 – NUMERICAL MODELLING

Computational simulations of the airflow over the double trailer truck models – were performed with the CFD program, Flo++ [35]. Since the version available for the simulations is designed for educational purposes, the simulations were limited to two dimensional flow caused by the constraint on the total number of cells that could be processed.

5.1 CONCEPT OF CFD

Computational Fluid Dynamics (CFD) uses numerical methods to explore the mechanics of fluids and the nature of their flow. With powerful graphics packages, CFD has become an important tool in the analysis of fluid flow problems. A general description of CFD can be found in reference [36].

To any fluid flow, conservation laws are applied with three extensive properties:

- The mass of the fluid
- The rate of change of momentum
- The rate of change of energy

The flow and its related phenomena are then described in the form of partial differential equations. The governing equations are analytically solvable only in a very small number of special cases of flow. Therefore, numerical methods are applied to approximate the exact results of the equations. The three numerical methods often used in CFD are Finite Element, Finite Difference and Finite Volume.

5.1.1 MASS CONSERVATION

The mass conservation equation (continuity) equation for an unsteady, compressible flow is given by,

$$\frac{\partial \rho}{\partial t} + \frac{\partial(\rho u)}{\partial x} + \frac{\partial(\rho v)}{\partial y} + \frac{\partial(\rho w)}{\partial z} = 0$$

where u is the velocity component in the x-direction and v and w the components in the y- and z- directions respectively, t is the time and ρ the density of the fluid. The continuity equation can be simplified in a differential coordinate-free form,

$$\frac{\partial \rho}{\partial t} + \mathrm{div}(\rho U) = 0 \qquad (5.1)$$

For an incompressible flow, the density of the fluid is constant, and the equation can be written as

$$\mathrm{div}\, U = 0 \qquad (5.2)$$

where U is the velocity vector.

5.1.2 MOMENTUM CONSERVATION

In the momentum equations, two types of forces are involved: surface forces and body forces. Surface forces include pressure and shear stresses, and the typical body forces are gravity and centrifugal force. For an incompressible flow, the momentum equations in Cartesian coordinates are given by,

$$\rho\frac{du}{dt}=\frac{\partial(-p+\tau_{xx})}{\partial x}+\frac{\partial\tau_{yx}}{\partial y}+\frac{\partial\tau_{zx}}{\partial z}+S_{Mx} \qquad (5.3)$$

$$\rho\frac{dv}{dt}=\frac{\partial(-p+\tau_{yy})}{\partial y}+\frac{\partial\tau_{xy}}{\partial x}+\frac{\partial\tau_{zy}}{\partial z}+S_{My} \qquad (5.4)$$

$$\rho\frac{dw}{dt}=\frac{\partial(-p+\tau_{zz})}{\partial z}+\frac{\partial\tau_{xz}}{\partial x}+\frac{\partial\tau_{yz}}{\partial y}+S_{Mz} \qquad (5.5)$$

where S_{Mi} is a source of a unit momentum in i-direction, and τ_{ji} is the shear stress on the ji-plane in the i-direction.

5.1.3 NAVIER-STOKES EQUATIONS

The continuity plus momentum equations are called the Navier-Stokes equations (NSE). For the finite volume method used in Flo++, these equations can be written in the form:

$$\rho\frac{du}{dt}=-\frac{\partial p}{\partial x}+\mathrm{div}(\mu\,\mathrm{grad}\,u)+S_{Mx} \qquad (5.6)$$

$$\rho\frac{dv}{dt}=-\frac{\partial p}{\partial y}+\mathrm{div}(\mu\,\mathrm{grad}\,v)+S_{My} \qquad (5.7)$$

$$\rho\frac{dw}{dt}=-\frac{\partial p}{\partial z}+\mathrm{div}(\mu\,\mathrm{grad}\,w)+S_{Mz} \qquad (5.8)$$

where μ is the dynamic viscosity of the fluid.

5.2 SOFTWARE

The software for the simulation in this thesis is a commercial software package: Flo++, version 2.3 for educational purposes. Flo++ is a computational fluid dynamics program for the solution of fluid flow and heat transfer problems. The numerical method applied by Flo++ is Finite Volume. It solves the basic conservation equations of fluid dynamics and produces results for velocities, pressures, temperatures and other flow variables.

5.3 SIMULATION PROCEDURE

Usually, a CFD package consists of three parts: Pre-processor, Solver and Post-processor. The pre-processor and post-processor are user interfaced.

In the pre-processor, the dimensions of the flow domain that simulate the physical model are defined, then divided into a number of cells. After the grid generation, the boundary conditions of the grid must be specified. The fluid properties such as density, velocity and viscosity are then entered. The type of fluid flow is defined by setting turbulence models and the options of steady or unsteady flow. Here, the control parameters for the solver are specified, in particular the convergence level.

The solver firstly establishes the initial model of the flow through reading the input file from the pre-processor. A set of algebraic equations to approximate the governing equations for the particular case of flow are created and solved. The computation stops when the resultant error level is below the convergence level, or after the number of specified global iterations are completed. The computational results for every cell and vertex are saved in an output file.

The post-processor presents the results in the form of graphical images, while the results for the calculated parameters such as velocity, pressure, temperature etc. can be printed out in coloured plots, which are easy to interpret.

5.3.1 MESH GENERATION

Modelling a fluid flow in CFD begins by defining the overall size and shape of the flow domain. Once the geometrical extent of the domain is established, the domain is represented by many small cubic cells. The domain is usually generated in three dimensions. However for the numerical model in this thesis,

the mesh was limited to two dimensions, due to the limitation of the maximum number of cells for the version of Flo++ available.

A special technique, Mesh Embedding is implemented to refine cells locally in regions where a high flow resolution is required. For the simulation of the airflow over a commercial truck, two regions with different density of mesh cells, coarse and fine grid areas were constructed respectively. Then they are incorporated together using the mesh embedding method.

5.3.2 BOUNDARY CONDITIONS

Once the mesh has been generated, the boundary conditions are defined. These boundary conditions include:

- The *inlet* boundary condition: the boundary where the distribution of velocity, density, temperature, concentration, etc., are known
- The *outlet* boundary condition: at this boundary, zero gradients of velocity are imposed while other variables are extrapolated from the interior. More than one boundary can be set as an outlet boundary condition provided that the mass fraction for each outlet is known.
- The *wall* boundary condition: at a wall boundary, the velocity normal to the boundary surface is zero. The default velocity tangential to the wall is also zero. However the wall can be given a velocity.
- The *pressure* boundary condition: the boundary where the static pressure distribution is known but the velocity will be determined.
- The *symmetry* boundary condition: the normal velocity on this boundary is zero and the normal gradients of all other variables are zero.

Four boundary conditions were applied in the numerical modelling of this thesis: inlet, outlet, symmetry and wall, which acted on the left, right, top and bottom surfaces of the airflow domain respectively. In order to represent the relative motion between the truck and road, the wall was set with a velocity of 22 m/s.

5.3.3 SOLUTION CONTROL

The equations, mentioned in section 5.1, are discretised by a discretization scheme, such as Upwind Differencing (UD), Centre Differencing (CD), Quadratic upwind interpolation (QUICK) etc. Once the discretisation process has been effected, a system of linear algebraic equations is solved. In this particular application, the upwind scheme was chosen because the Peclet number has a value greater than 2, avoiding the instabilities of the central difference scheme.

Two important parameters that are used to control the iterative solution are the number of global iterations that will be performed and the overall convergence level. The solution automatically stops when the error level in the solution is below the overall convergence level, or the number of specified iterations is completed.

A solution to a specified flow problem and its associated boundary conditions is obtained through a series of steps called global iterations. In each global iteration, a system of the linear algebraic equations is solved for the flow variables, such as the components of velocity, pressure, temperature etc. The solution of each individual system involves a series of inner iterations called sweeps.

The other parameters for solution control include the relaxation and residual levels. The range of relaxation is from 0.2 to 1.4. A default value of 0.7 for steady flows is set in Flo++. The default residual value is 0.1 and is only altered for unsteady flow.

5.4 NUMERICAL RESULTS

The numerical results of the simulation of the scaled truck models are presented in this section. All the codes of pre-processing files are shown in Appendix C,

including a general post-processing file.

Each simulation was performed at an air velocity of 22 m/s. other parameters for the simulations are set as follows:

Density:	1.205	kg/m^3
Viscosity:	1.85×10^{-5}	m^2/s
Pressure:	100000	Pa (Reference Pressure)

The steady flow is incompressible and turbulent. The turbulence model is the standard k-ε model for high Reynolds numbers. The convergence level has the value of 0.001.

For numerical simulations, all the truck models have no wheels. Following the simulation of the flow over the original truck model, models with various combinations of add-on devices are investigated. The add-on devices used in the numerical modelling include front fender, rear fender, gap seals, cab roof deflector and rear cavities.

5.4.1 FLOW DOMAIN AND TRUCK MODELS

The flow domain for all the simulations was 2.2 m in the x-direction, 0.8 m and 0.01 m in y and z directions respectively. The free stream velocity was in the positive x-direction. The domain is divided into two areas: a coarse grid area and a fine grid area, with the model in the fine grid area. The domain size and the position of the original truck model are shown in Figs. 5.1 and 5.2. The total number of cells for each simulation is 8240.

The geometry of the add-on devices is constructed by using cells. Therefore the shape and size of the devices are constrained by the shape and size of a single cell. The add-on devices are shown in Figs. 5.3 to 5.5.

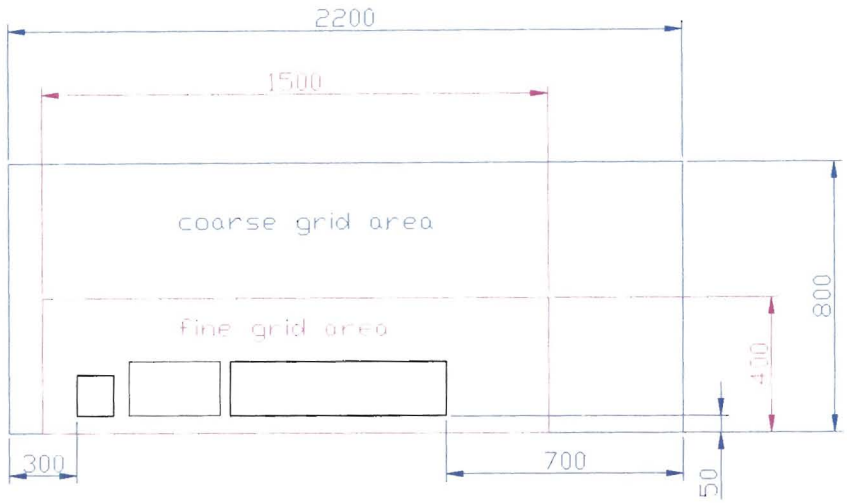

Fig. 5.1: Flow domain and the original model

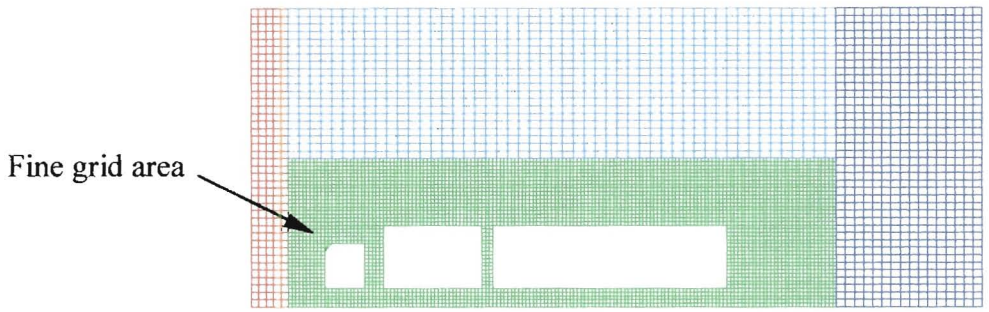

Fig. 5.2: Coarse grid and fine grid areas

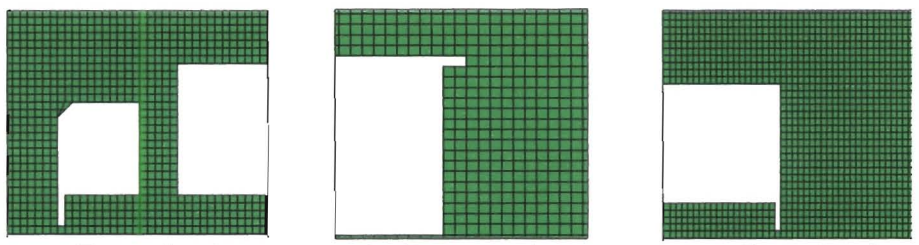

a: Front fender b: Rear cavity c: Rear fender

Fig. 5.3: Models with add-on devices

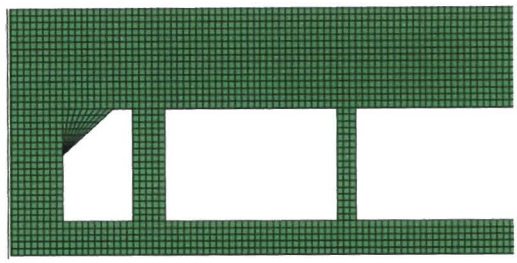

Fig. 5.4: Model with a cab deflector

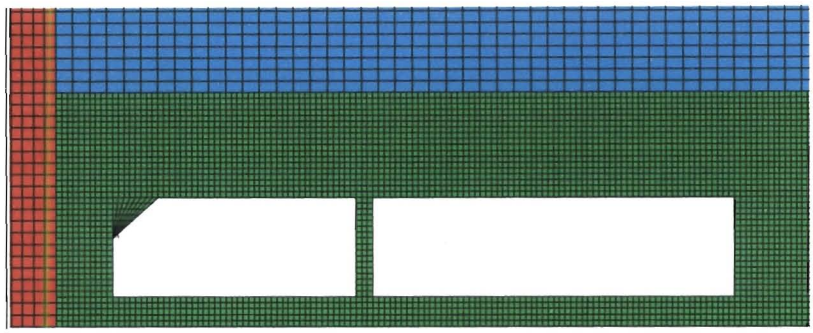

Fig. 5.5: Model with no gap

5.4.2 CHARACTERISTICS OF VELOCITY VECTORS

From Figs. 5.6 – 5.9, it is clearly seen that the air velocity above the model is increased as the air is deflected. It is also seen that there is a boundary flow above each model. The model with no gap between cab and trailer gave the lowest increase in air velocity. The shape of the model with a cab deflector and no gap between cab and trailer is almost similar to that which some researchers suggest for a future innovative truck design [37].

In the wake of the models, there is a recirculating flow. The flow is symmetric about the horizontal centre line of the rear face, indicating that with a high ground clearance, the model is so far from the ground that the effect of the road is negligible.

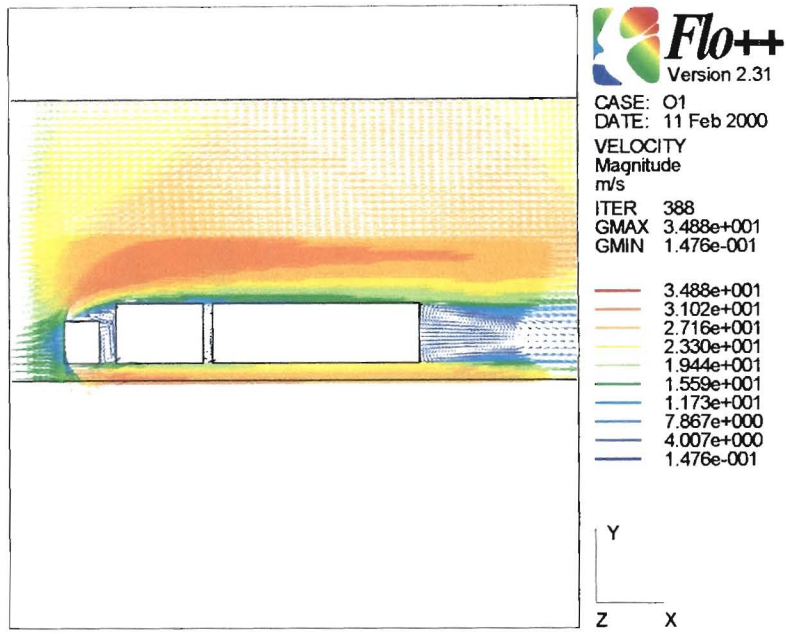

Fig. 5.6: Computational velocity vectors
for the basic model (no add-on devices)

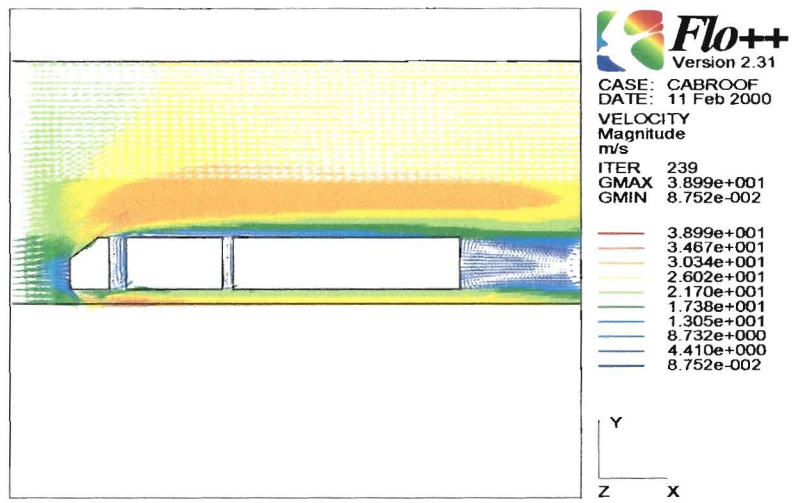

Fig. 5.7: Computational velocity vectors
for the model with cab deflector

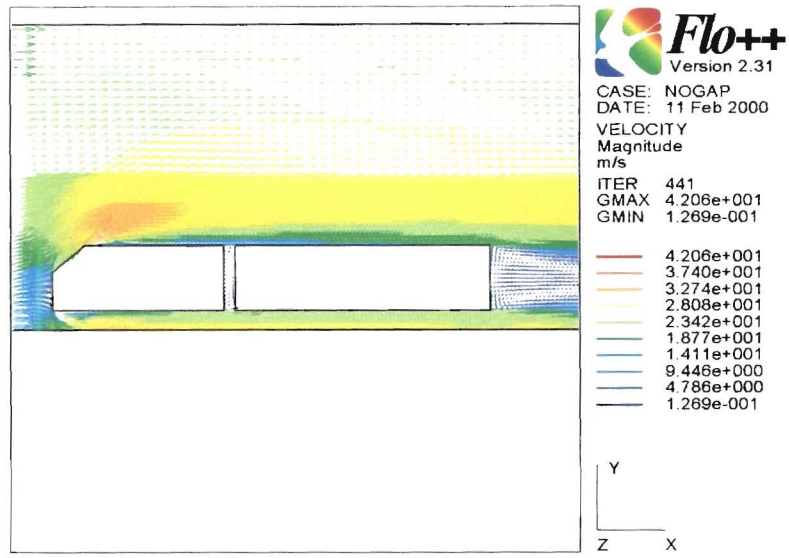

Fig. 5.8: Computational velocity vectors
with no gap between cab and trailer

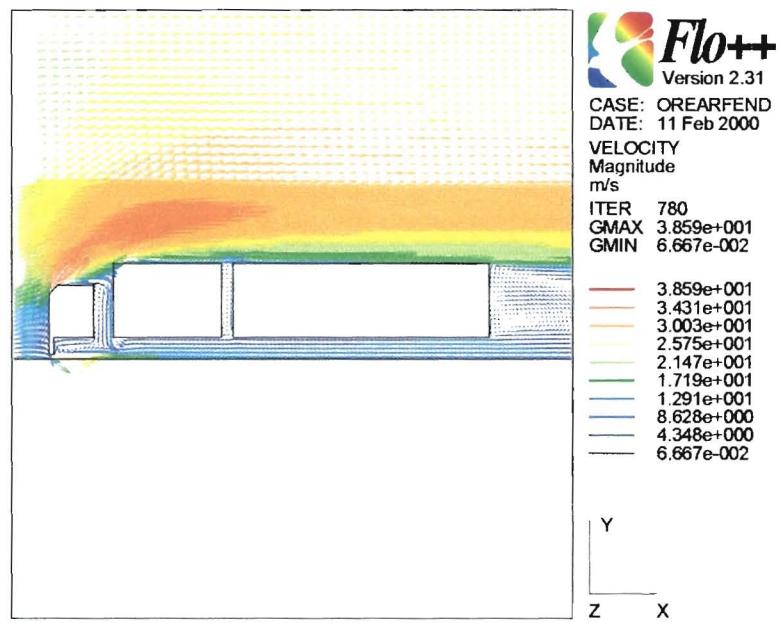

Fig. 5.9: Computational velocity vectors
For the model with the front fender

5.4.3 PRESSURE DISTRIBUTIONS

The pressure coefficient curves in Fig. 5.10 clearly show that adding either a cab roof deflector or front fender can decrease the pressure on the front vertical face of the front trailer. The pressure on the low part of the surface remains fairly constant for the basic model and the model with a front fender. This may be due to the fact that the simulation is in two dimensions.

For the basic model, the pressure on the front vertical face of the front trailer is negative with respect to the reference pressure (100000 Pa), which is different from the experimental result (Fig. 4.8a), and is also probably due to the 2-D limitation of Flo++. Fig.5.11b shows that the area of flow stagnation in front of the tractor is increased when the front fender is added. It can be observed from Fig. 5.11c that the addition of the cab deflector removes the pressure bubble on the top forward edge of the front trailer, which is consistent with the results of the wind tunnel tests (Fig. 4.3b).

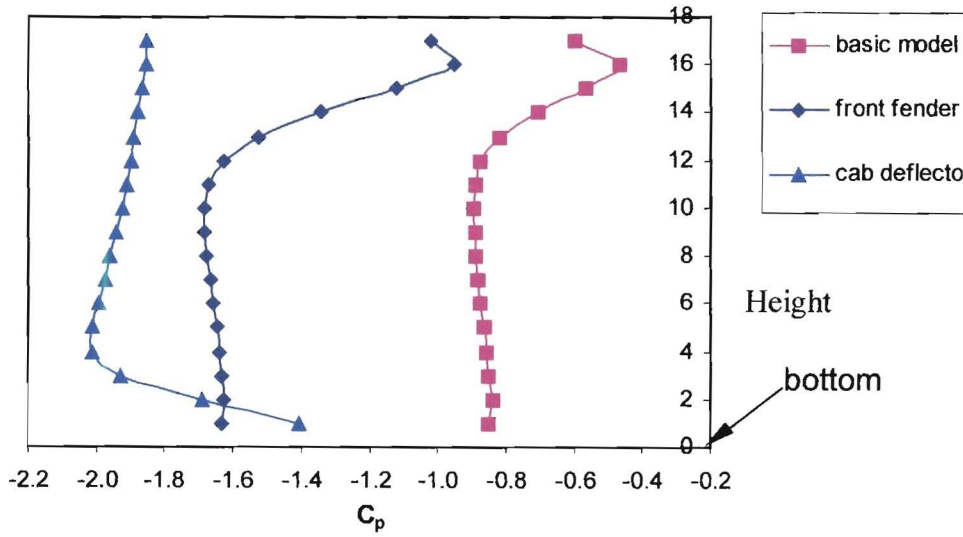

Fig. 5.10: Pressure distributions on the front face of the front trailer

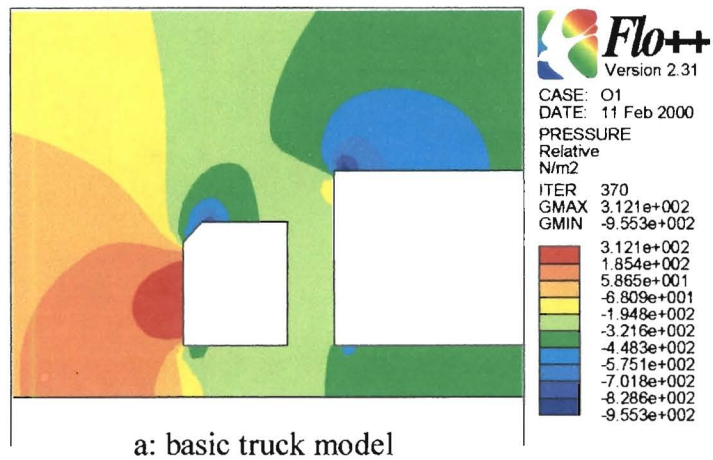

a: basic truck model

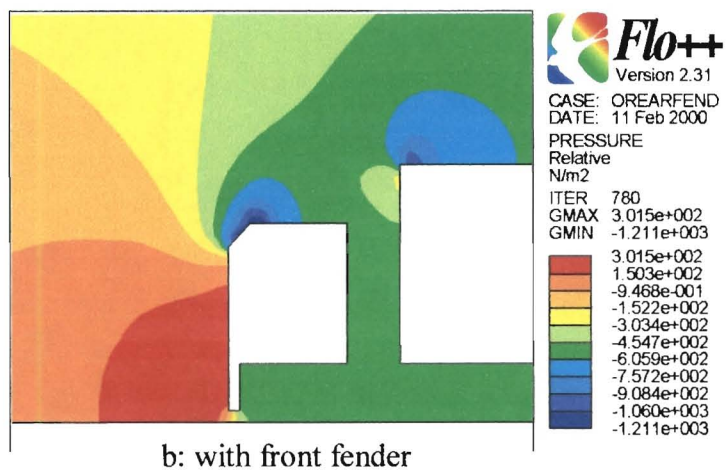

b: with front fender

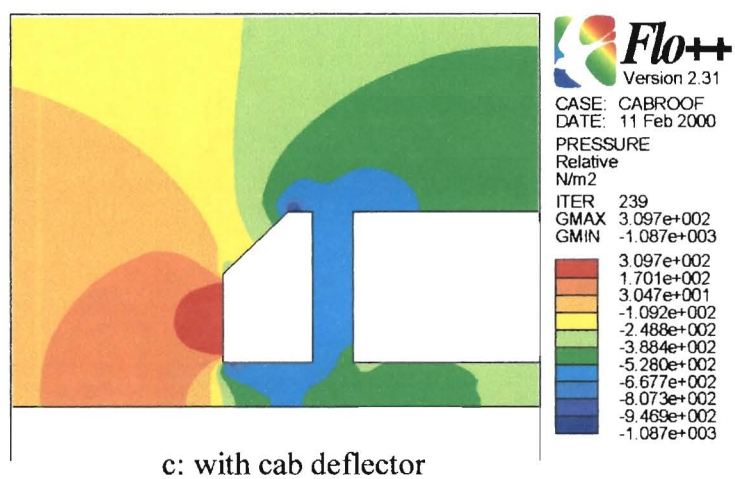

c: with cab deflector

Fig. 5.11: Pressure contours on models

The pressure distribution on the back face of the rear trailer for the basic model is symmetrical about the horizontal centre line (Fig. 5.13a). The pressure in the central region is greater than those at both upper and lower regions of the surface, resulting in flow recirculation. In Fig. 5.12, it is seen that adding the rear fender significantly reduced the pressure on the back face of the rear trailer. The edge cavity also gave a decrease in pressure. Both of these devices would therefore contribute to a drag increase.

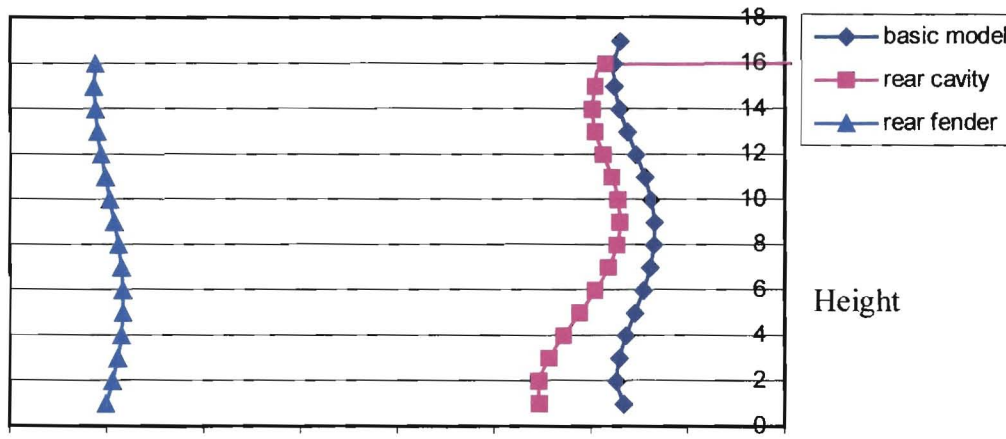

Fig. 5.12: Pressure distribution on the rear face of the rear trailer

5.4.4 DRAG FORCES

The drag coefficients for some computational models are listed in Table 7. It is clearly seen that only the model with a cab deflector and gap seal has a drag coefficient less than that of the basic model.

Table 7 Computational drag coefficients at V = 22 m/s

Model	Basic model	cab deflector	front fender	rear cavity	rear fender	CD+ gap seal
C_D	0.9335	0.9808	1.7334	0.9479	2.3387	0.8049

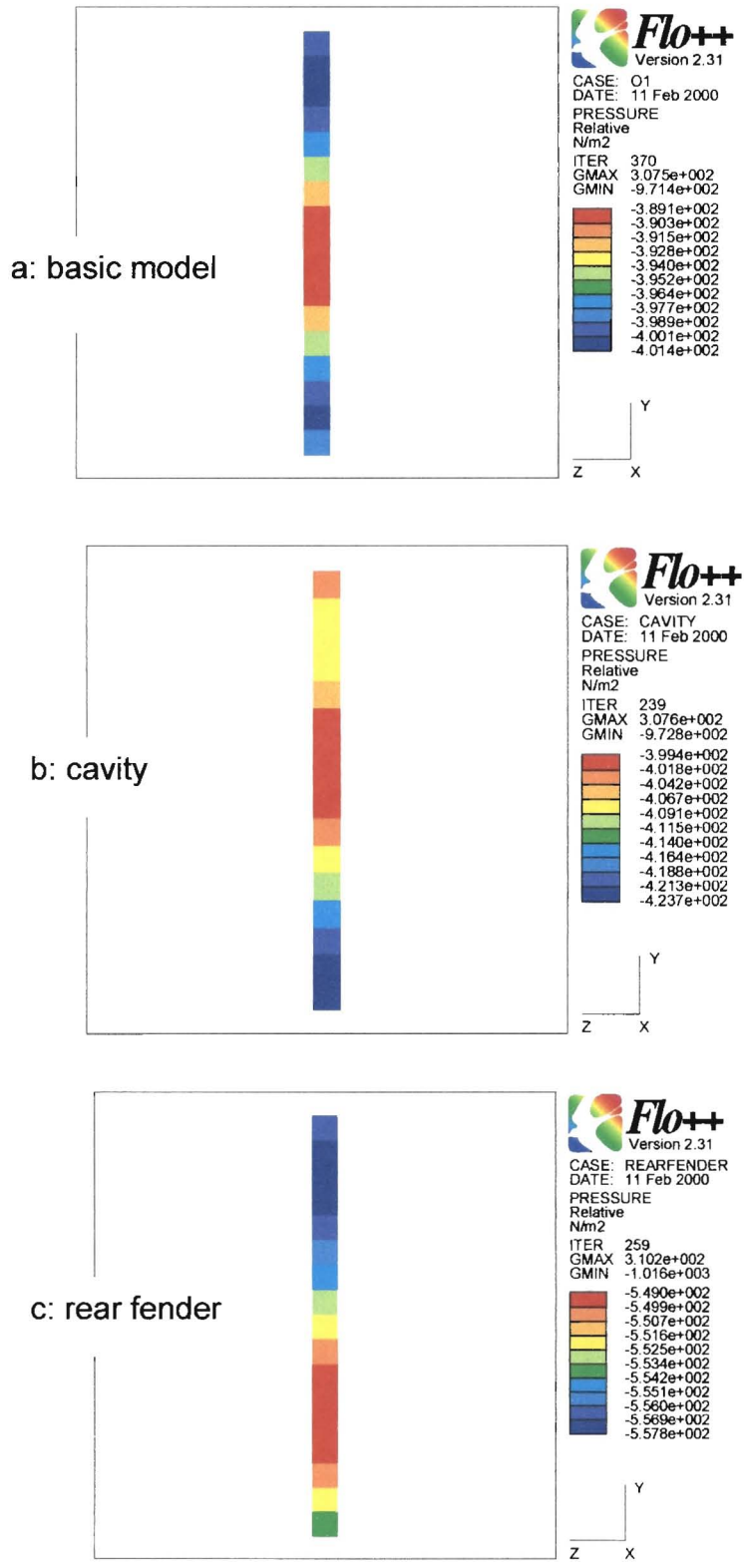

Fig. 5.13: Pressure contours on the rear face of the rear trailer

5.5 LIMITATION OF THE NUMERICAL METHOD

Since the numerical simulations performed in this thesis are limited to two dimensions, the results of the numerical modelling of the truck show some significant differences from the experimental results. Actually, the drag coefficients listed in Table 7 did not act on the whole frontal area of a real truck in 3-dimensions. Thus the numerical results are not a good representation of the drag characteristics of the real truck. This implies that for the truck aerodynamic study the numerical model must be built using a three dimensional model. What the numerical model does indicate however, is the probable flow regime around the truck and areas of flow separation, reattachment and wake formation.

CHAPTER 6 - CONCLUSIONS

Based on the results of both the wind tunnel experimental tests and computational simulations, the following conclusions concerning the aerodynamic characteristics of the double trailer truck model and the corresponding drag reduction techniques may be drawn:

At a Reynolds number of 1.6×10^5 and a yaw angle of zero degrees, the drag coefficient of the original truck model is 0. 9283. A 26% reduction in C_D was obtained due to the addition of the cab deflector. Further adding either center or side gap seals did not give an extra drag reduction. However, with the cab deflector and side skirts already mounted on the model, a 28% and 30% drag reduction were obtained by the addition of center and side gap seals respectively. The drag increase or decrease caused by fitting rear face fairings lay within $\pm$ 7% depending upon the fitting concerned.

At a yaw angle of 5^0, the drag coefficient of the original truck model increases by about 18%, from 0.9283 to 1.088. The drag reduction due to adding the cab deflector is 8.4%, much less than the 26% drag reduction at zero yaw. The effectiveness of a cab roof deflector in reducing drag decreases when the yaw angle increases. The largest drag reduction of 29% was achieved with a combination of the cab deflector, side skirts and side gap seals. Side gap seals have an influence on the airflow under the truck body by decreasing the amount of air flowing down through the gap, especially at crosswind conditions. The addition of side skirts alone gave a 6% reduction in C_D at a yaw angle of 5^0, a little more than 4% drag reduction at zero yaw.

The drag coefficients for all the truck models tested in the wind tunnel experiments are approximately constant for Reynolds numbers above 1.65×10^5 at both 0^0 and 5^0 yaw angles.

The pressure on the front vertical face of the front trailer was considerably decreased by the addition of the cab deflector at zero yaw. Fitting guide vanes on the rear edge of the rear trailer results in a decrease in pressure on the rear vertical face of the trailer, while the pressure on the same surface is increased due to the addition of either rear cavities or edge fairings.

From the results of both the wind tunnel experiments and numerical simulations, it is suggested that for a future truck design, the gap between the cab and the trailer should be removed.

CHAPTER 7 - REFERENCES

1. Drollinger, R.A., *"Heavy Duty Truck Aerodynamics"*, SAE 87001, 1987.
2. Modi, V.J., Hill and S.St., Yokomizo, T., *"Drag Reduction for Trucks Through Boundary Layer Control"*, Journal of Wind Engineering and Industrial Aerodynamics Vol. **54/55,** 1995, pp. 265-274.
3. Garry, K.P., *"A Review of Commercial Vehicle Aerodynamic Drag Reduction Techniques"*, Proc. Instn. Mech. Engrs., Vol.**199**, 1985, pp. 215-220.
4. Miles, A.W., *"Drag reduction of HULTRAN truck trailer combination"*, Engineering Research, (PTY) LTD, Report No. HU/1, 1978.
5. Mason, W.T. and Beebe, P. S., *"The drag related flow field characteristics of trucks and buses"*, Aerodynamic Drag Mechanisms of Bluff Bodies and Road Vehicles, General Motors Research Laboratories Symposium, Plenum, New York, 1978, pp. 45-90.
6. Hucho, W.H. and Sovran, G., *"Aerodynamics of road vehicles"*, Annu.Rev. Fluid Mech. Vol. **25**, 1993, pp. 485-537.
7. Marks, C.H., Buckley, F.T. and Walston, W.H., *"An evaluation of the aerodynamic drag reductions produced by various cab roof fairings and a gap seal on tractor-trailer trucks"*, SEA 760105, 1976.
8. Lajos, T., Preszler, L. and Finta. L., *"Styling and aerodynamics of buses"*, Int. J. of Vehicle Design, Vol. **9**, 1988, pp. 1-15.
9. Bearman, P.W., "*Review - bluff body flows application to vehicle aerodynamics*", Journal of Fluids Engineering, Vol.**102**, 1980, pp. 265 - 274.
10. Gilhaus, A., *"The influence of cab shape on the air drag of trucks,"* Journal of Wind Engineering and Industrial Aerodynamics,Vol. **9**, 1981, pp. 77 - 87.
11. Craig, K.J., Snyman, J.A., Thirion, F.J. and Stander, N., *"Drag minimisation of bluffbody shapes using CFD and mathematical optimisation"*, Proceedings of the1st South African Conference on Applied Mechanics (SACAM) '96, Midrand, South-Africa, 1-5 July, 1996.

12. Modi, V.J., Ying, B. and Yokomizo, T., *"An approach to design of the next generation of fuel efficient trucks through aerodynamic drag reduction"*, Advanced Automotive Technologies, DE-Vol. **40** ASME 1991.
13. Bettes, W.H., Discussion. Aerodynamic Drag Mechanisms of Bluff Bodies and Road Vehicles, General Motors Research Laboratories Symposium, Plenum, New York, 1978, pp. 93.
14. Garry, K.P., *"Development of container-mounted devices for reducing the aerodynamic drag of commercial vehicles"*, Journal of Wind Engineering and Industrial Aerodynamics, Vol. **9**, 1981, pp. 113-124.
15. Buckley, F.T. and Sekscienski, W.S., *"Comparisons of effectiveness of commercially available devices for the reduction of aerodynamic drag on tractor-trailers"*, SAE 750704, 1975.
16. Garry, K.P., *"Wind tunnel techniques for reducing commercial vehicle Aerodynamic drag"*, CoA Report 8220, Cranfield College of Aeronautics, September, 1982.
17. Marks, C.H. and Buckley, F.T., *"The effect of tractor-trailer flow interaction on the drag and distribution of drag of tractor-trailer trucks"*, SAE 801403, 1980.
18. Buckley, F.T., Marks, C.H. and Walston, W.H., *"Analysis of coast-down data to assess the aerodynamic drag reduction on full-scale tractor-trailer trucks in windy environments"*, SAE 760850, 1976.
19. *"AirTabs"*, Website: www.airtab.com.
20. Holmes, H.R., *"Practical economic aspects of tractor/trailer aerodynamics"*, SAE 760103, 1976.
21. Fujimoto, T., Miyake, N., Watanabe, Y. and Takeyama, T., *"Suppression of mud adhesion to the rear surface of a van-type truck"*, SAE 920203, 1992.
22. Kirsch, J.W., Garg, S.K. and Bettes, W., "*Drag reduction of bluff vehicles with airvanes*", SAE 730686, 1973.

23. Steers, L.L., Montoya, L.C. and Saltzman, E.J., *"Aerodynamic drag reduction tests on a full-scale tractor-trailer combination and a representative box-shaped ground vehicle"*, SAE 750703, 1975.
24. SAE Recommended Practice, *"Wind tunnel test procedures for trucks and buses"*, SAEJ1252, 1968.
25. Saunders, J.W., Watkins, S., Hoffmann, P.H. and Buckley, F.T., *"Comparison of on-road and wind tunnel tests for tractor-trailer aerodynamic devices, and fuel saving predictions"*, SAE 850286, 1985.
26. Olson, M.E. and Schaub, U.W., *"Aerodynamics of trucks in wind tunnels: the importance of replicating model form and detail, cooling system and test conditions"*, SAE 920345,1992.
27. Lutz, T., *"The effect of the boundary layer present in wind tunnels on the aerodynamic drag of a model truck"*, MSc thesis, University of Cape Town, South Africa, 1997.
28. Cooper, K.R., Mason, W.T. and Bettes, W.H., "*Correction experience with the SAE wind tunnel test procedure for trucks and buses"*, SAE 820375, 1982.
29. Garry, K.P., *"Some effects of ground clearance and ground plane boundary layer thickness on the mean base pressure of a bluff vehicle type body"*, Journal of Wind Engineering and Industrial Aerodynamics, Vol. **62**, 1996, pp. 1-10.
30. Burgin, K., Adey, P.C. and Beatham, J.P., "*Wind tunnel tests on road vehicle models using a moving belt simulation of ground effect"*, Journal of Wind Engineering and Industrial Aerodynamics, Vol. **22**, 1986, pp. 227-236.
31. Matsunaga, K., Miyata, H., Aoki, K. and Zhu, M., "*Finite-difference simulation of 3D vortical flows past road vehicles"*, SAE 920339,1992.
32. Hirt, C.W. and Ramshaw, J.D., *"Prospects for numerical simulation of bluff-body aerodynamics"*, Aerodynamic Drag Mechanisms of Bluff Bodies and Road Vehicles, General Motors Research Laboratories Symposium, Plenum, New York, 1978, pp. 227-246.

33. SAE information report, "*Aerodynamic testing of road vehicles*", SAEJ2071, 1990.
34. Pope, A. and Harper, J.J., "Low-speed wind tunnel testing", Wiley, New York, 1966.
35. "Flo++", Website: www.softflo.com
36. Ferziger, J.H. and Peric, M., "Computational methods for fluid dynamics", Springer, New York, 1997.
37. Siuru, B., "Technology keeps 18 – wheelers truck in", Mechanical Engineering August, 1988, pp. 30-33.

APPENDIX A – EXPERIMENTAL DATA

In this appendix, the wind tunnel experimental results are presented in terms of drag force and pressure coefficient in tables. The acronym used in the tables are listed below:

- CD – Cab Deflector

- SS – Side Skirts

- RF -- Rear Fender

- SGS – Side Gap Seal

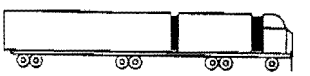

- CGS -- Center Gap Seal

- GV -- Guide Vanes

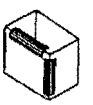

- EF -- Edge Fairings

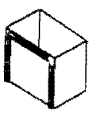

- RC -- Rear Cavities

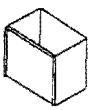

Table 1. Drag forces of truck models at $\beta = 0^0$

		Drag force D (N)							
	V (km/h) / model	40	50	60	70	80	90	100	110
1	Original truck	1.88	2.92	4.14	5.90	7.72	9.78	12.18	14.62
2	Cab Deflector (CD)	1.38	2.12	2.98	4.30	5.66	7.16	8.94	10.82
3	Side Skirts (SS)	1.84	2.78	4.02	5.62	7.40	9.40	11.64	14.12
4	Guide Vanes (GV)	2.00	3.10	4.36	6.20	8.12	10.30	12.84	14.84
5	Rear Cavities (RC)	1.86	2.84	4.02	5.78	7.54	9.58	11.94	13.76
6	Edge Fairings (EF)	1.86	2.88	4.08	5.82	7.34	9.70	11.46	13.84
7	Rear Fender (RF)	1.98	3.06	4.42	6.20	8.16	10.30	12.78	15.48
8	CD + CGS	1.40	2.18	3.00	4.40	5.72	7.24	8.94	10.82
9	CD + SGS	1.42	2.14	3.06	4.32	5.64	7.18	8.96	10.64
10	CD + SS	1.40	2.10	2.94	4.24	5.56	7.06	8.76	10.56
11	CD + GV	1.62	2.42	3.44	4.90	6.42	8.18	10.04	12.14
12	CD + RC	1.40	2.12	3.00	4.28	5.64	7.18	8.84	10.68
13	CD + EF	1.42	2.16	3.08	4.36	5.78	7.28	9.00	10.84
14	CD + RF	1.62	2.40	3.36	4.94	6.52	8.14	9.98	12.06
15	CD + FRONT SGS	1.40	2.16	2.98	4.38	5.72	7.22	8.88	10.74
16	CD + FRONT CGS	1.42	2.14	3.06	4.30	5.68	7.16	8.92	10.74
17	CD + SS + GV	1.56	2.38	3.36	4.78	6.38	8.02	9.94	12.06
18	CD + SS + RC	1.36	2.08	2.92	4.22	5.54	7.00	8.70	10.48
19	CD + SS + EF	1.36	2.06	2.88	4.18	5.50	6.98	8.64	10.38
20	CD + SS + RF	1.40	2.16	2.98	4.36	5.72	7.18	8.94	10.76
21	CD + CGS + SS	1.40	2.08	2.94	4.26	5.56	7.06	8.74	10.52
22	CD + SGS + SS	1.32	2.00	2.80	4.10	5.40	6.78	8.42	10.18

Continued Table 1.

		Drag force D (N)							
	V (km/h) / Model	40	50	60	70	80	90	100	110
23	CD + CGS + GV	1.56	2.46	3.36	4.82	6.44	8.12	10.04	12.14
24	CD + CGS + RC	1.40	2.18	3.00	4.36	5.70	7.20	8.94	10.86
25	CD + CGS + EF	1.44	2.18	3.08	4.34	5.70	7.24	8.90	10.76
26	CD + SGS + GV	1.56	2.38	3.34	4.80	6.30	7.98	9.84	11.90
27	CD + SGS + RC	1.38	2.10	2.96	4.26	5.54	7.06	8.70	10.50
28	CD + SGS + EF	1.40	2.08	2.94	4.30	5.64	7.08	8.74	10.62
29	CD + RF + RC	1.56	2.36	3.38	4.90	6.32	8.08	9.90	11.98
30	CD + RF + EF	1.62	2.40	3.42	4.90	6.42	8.06	10.02	12.06
31	CD + RF + GV	1.72	2.62	3.68	5.32	6.94	8.74	10.90	13.06
32	CD + CGS + SS + GV	1.56	2.38	3.32	4.84	6.28	8.02	9.90	11.98
33	CD + CGS + SS +RC	1.38	2.06	2.92	4.22	5.48	6.94	8.62	10.46
34	CD + CGS + SS +EF	1.38	2.08	2.88	4.20	5.50	6.98	8.60	10.40
35	CD + SGS + SS +GV	1.52	2.32	3.28	4.68	6.16	7.78	9.66	11.68
36	CD + SGS + SS +RC	1.32	2.00	2.78	4.06	5.30	6.72	28.04	10.04
37	CD + SGS + SS +EF	1.32	2.00	2.80	4.10	5.36	6.76	8.42	10.12
38	CD + SS + RF + GV	1.58	2.42	3.38	4.88	6.36	8.10	10.00	12.06
39	CD + SS + RF + RC	1.42	2.12	2.98	4.34	5.70	7.22	8.90	10.76
40	CD + SS + RF + EF	1.38	2.08	2.96	4.32	5.64	7.18	8.88	10.72

Table 2. Drag forces of truck models at $\beta = 5^0$

		Drag force D (N)							
	V (km/h) / model	40	50	60	70	80	90	100	110
1	Original truck	2.27	3.45	4.94	6.95	9.05	11.50	14.27	17.21
2	Cab Deflector	2.11	3.21	4.46	6.30	8.29	10.54	13.05	15.72
3	Side Skirts	2.11	3.21	4.62	6.48	8.51	10.74	13.29	16.06
4	CD + CGS	1.79	2.77	3.91	5.60	7.31	9.26	11.42	13.79
5	CD + SGS	1.81	2.79	3.94	5.58	7.29	9.26	11.44	13.77
6	CD + SS	1.97	3.03	4.26	6.02	7.99	10.10	12.47	15.00
7	CD + SS + SGS	1.61	2.47	3.49	4.88	6.42	8.17	10.10	12.19
8	CD + SS + CGS	1.69	2.55	3.69	5.24	6.83	8.69	10.88	13.31
9	CD + FRONT SGS	1.83	2.79	3.94	5.54	7.29	9.24	11.42	14.05
10	CD + FRONT CGS	1.81	2.79	3.98	5.60	7.37	9.28	11.52	13.99

Table 3. Pressure coefficients on the front face of the front trailer

V = 80 km/h

	Original Truck	Cab Deflector	CD + CGS	CD + SGS
point 1	0.8116	-0.2860	-0.2860	-0.3393
point 2	0.1996	-0.2262	-0.2129	-0.3592
point 3	-0.1730	-0.2661	-0.2594	-0.3193
point 4	-0.0437	-0.3326	-0.3193	-0.2727
point 5	0.4524	-0.2794	-0.2528	-0.2461
point 6	0.8116	-0.2727	-0.2794	-0.3060
point 7	0.2395	-0.2528	-0.2727	-0.3659
point 8	-0.1863	-0.3060	-0.3193	-0.2993
point 9	-0.1330	-0.3725	-0.3925	-0.2794
point 10	0.2528	-0.3393	-0.3459	-0.2328
point 11	0.7450	-0.1197	-0.1131	-0.2860
point 12	0.3592	-0.2195	-0.2395	-0.3393
point 13	-0.1463	-0.3326	-0.3459	-0.2927
point 14	-0.2528	-0.3858	-0.3725	-0.2594
point 15	-0.2262	-0.3393	-0.3326	-0.2860

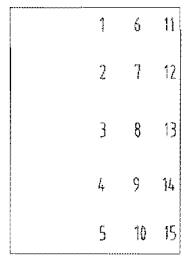

Table 4. Pressure coefficients on the front face of the rear trailer

V = 80 km/h

	Original Truck	Cab Deflector	CD + CGS	CD + SGS
point 1	-0.0806	-0.0030	-0.0148	-0.0961
point 2	-0.0178	0.0141	0.0208	-0.1377
point 3	-0.0329	0.0222	0.0057	-0.1117
point 4	-0.0450	0.0265	-0.0121	-0.0468
point 5	-0.0208	0.0243	0.0145	-0.0034
point 6	-0.0676	0.0110	-0.0578	-0.1169
point 7	0.0148	0.0222	0.0134	-0.1299
point 8	-0.0356	0.0075	-0.0165	-0.0468
point 9	-0.0511	0.0067	-0.0346	-0.0754
point 10	-0.0302	0.0164	-0.0145	-0.0260
point 11	0.1299	0.0524	0.0909	-0.1091
point 12	-0.0832	-0.0046	-0.0702	-0.1299
point 13	-0.0754	0.0100	-0.0572	-0.1013
point 14	-0.0474	0.0261	-0.0302	-0.0520
point 15	-0.0413	0.0257	-0.0326	-0.0387

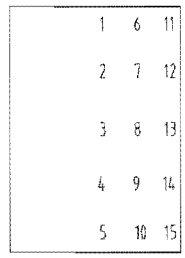

Table 5. Pressure coefficients on the rear face of the rear trailer

V = 80 km/h

	Original truck	Side Skirts	Guide Vanes	Rear Cavities	Lip Fairings	Rear Fender
point 1	-0.0457	-0.0484	-0.1065	-0.0312	-0.0356	-0.1221
point 2	-0.0754	-0.0585	-0.1247	-0.0624	-0.0676	-0.1273
point 3	-0.1091	-0.0858	-0.1351	-0.0987	-0.1039	-0.1221
point 4	-0.1091	-0.1065	-0.1325	-0.0987	-0.1091	-0.1143
point 5	-0.0909	-0.1013	-0.1195	-0.0806	-0.0884	-0.1039
point 6	-0.0416	-0.0468	-0.1013	-0.0338	-0.0364	-0.1221
point 7	-0.0728	-0.0546	-0.1247	-0.0624	-0.0650	-0.1247
point 8	-0.0961	-0.0754	-0.1299	-0.0884	-0.0909	-0.1143
point 9	-0.1117	-0.1117	-0.1247	-0.0987	-0.1091	-0.1143
point 10	-0.0961	-0.1013	-0.1117	-0.0806	-0.0909	-0.1065
point 11	-0.0416	-0.0442	-0.0884	-0.0312	-0.0286	-0.1117
point 12	-0.0702	-0.0572	-0.1585	-0.0598	-0.0598	-0.1195
point 13	-0.0961	-0.0832	-0.1273	-0.0884	-0.0961	-0.1169
point 14	-0.1117	-0.1091	-0.1221	-0.0987	-0.1065	-0.1117
point 15	-0.0961	-0.1039	-0.1819	-0.0806	-0.0987	-0.1117

Note: The tappings positions are the same as those in the front face of the rear trailer, seen in Table 4.

Table 6. Pressure coefficients on the top face of the front trailer

V = 80 km/h

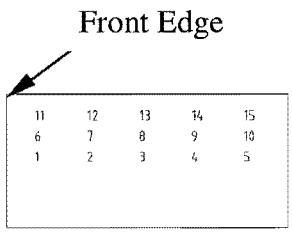

	Original Truck	Cab Deflector
point 1	-0.4573	-0.0370
point 2	-0.2806	-0.0380
point 3	-0.0363	-0.0258
point 4	-0.0064	-0.0158
point 5	-0.0267	-0.0264
point 6	-0.4781	-0.0512
point 7	-0.2962	-0.0426
point 8	-0.0365	-0.0287
point 9	-0.0102	-0.0190
point 10	-0.0231	-0.0148
point 11	-0.3274	-0.0489
point 12	-0.2651	-0.0667
point 13	-0.0122	-0.0272
point 14	-0.0095	-0.0154
point 15	-0.0225	-0.0102

Table 7. Pressure coefficients on the top face of the rear trailer

V = 80 km/h

	Original truck	Cab Deflector
point 1	0.0012	-0.0113
point 2	-0.0013	-0.0027
point 3	-0.0030	-0.0023
point 4	-0.0020	-0.0019
point 5	-0.0041	0.0027
point 6	-0.0004	-0.0008
point 7	-0.0024	-0.0042
point 8	-0.0082	-0.0103
point 9	-0.0145	-0.0176
point 10	-0.0094	-0.0145
point 11	-0.0155	-0.0211
point 12	-0.0161	-0.0235

	Original truck	Cab Deflector
point 13	-0.0009	-0.0112
point 14	-0.0022	-0.0036
point 15	0.0072	0.0067
point 16	-0.0013	-0.0003
point 17	0.0025	0.0036
point 18	0.0057	0.0041
point 19	-0.0010	-0.0015
point 20	-0.0084	-0.0097
point 21	-0.0091	-0.0101
point 22	-0.0145	-0.0167
point 23	-0.0124	-0.0160
point 24	-0.0253	-0.0283

	Original truck	Cab Deflector
point 25	0.0100	0.0030
point 26	0.0065	0.0049
point 27	-0.0025	-0.0007
point 28	-0.0048	-0.0036
point 29	0.0077	0.0077
point 30	0.0038	0.0036
point 31	-0.0031	-0.0036
point 32	-0.0180	-0.0194
point 33	-0.0188	-0.0209
point 34	-0.0155	-0.0181
point 35	-0.0168	-0.0196
point 36	-0.0097	-0.0124

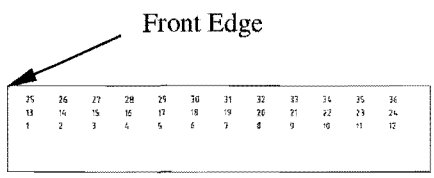

APPENDIX B – PHOTOGRAPHS OF MODELS

The important photographs of truck models taken in the experiments are presented in this appendix. They also include the photographs of flow visualisation.

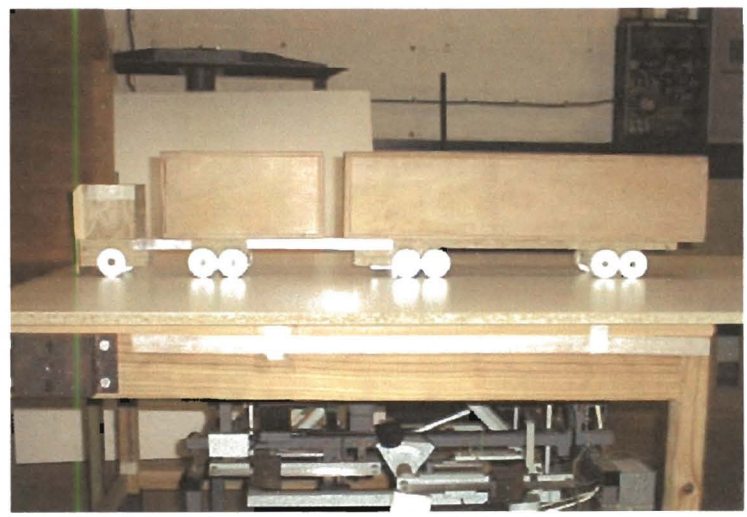

Figure B-1: Side view of the original model in the test section

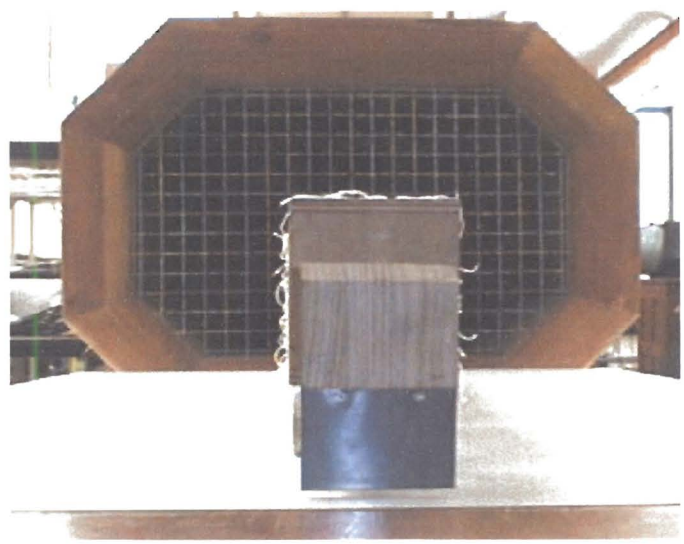

Figure B-2: Front view of the original model in the test section

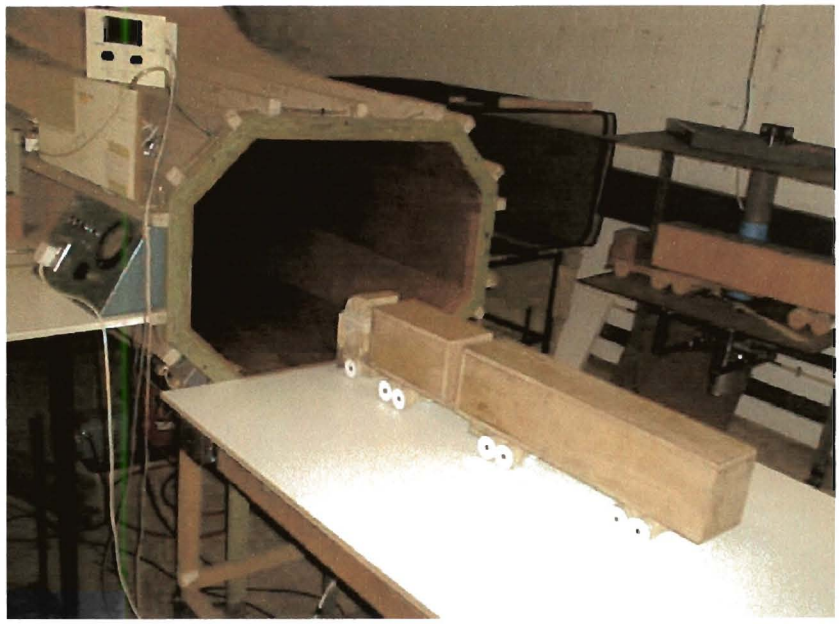

Figure B-3: Model with the cab roof deflector in the test section

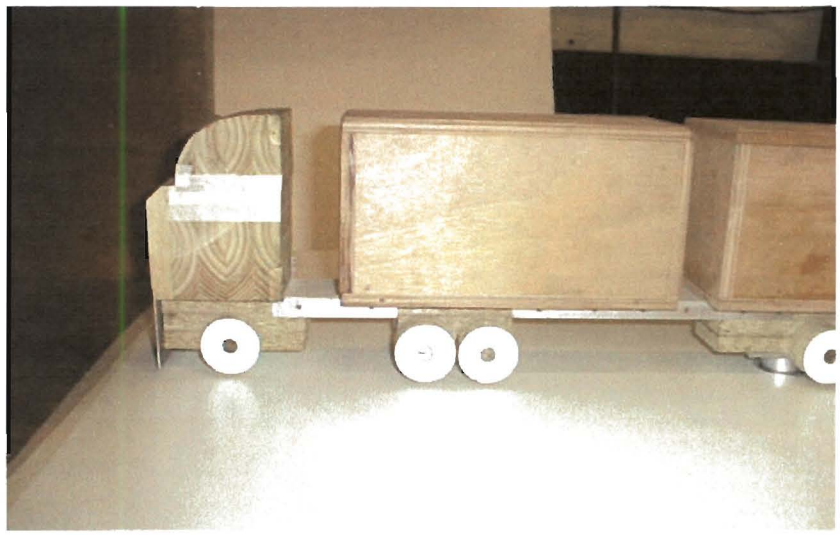

Figure B-4: Cab deflector Mounted on the cab roof

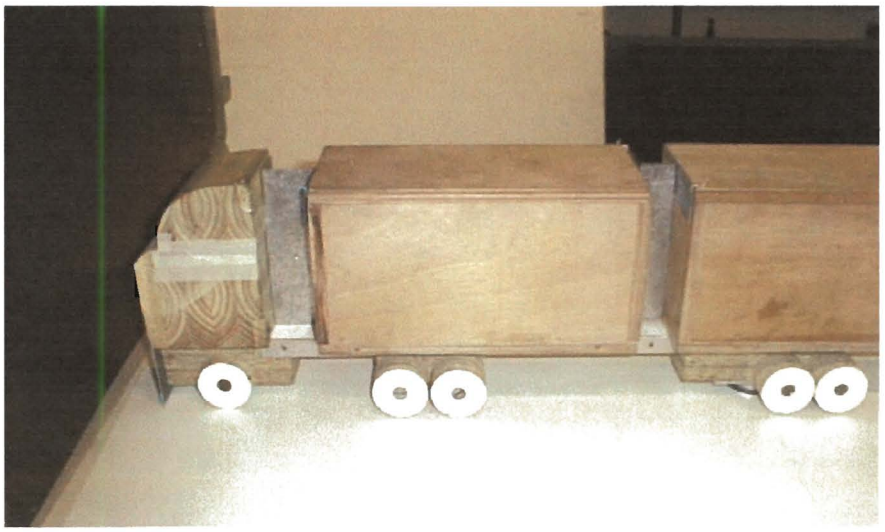

Figure B-5: Model with the cab deflector and centre gap seals

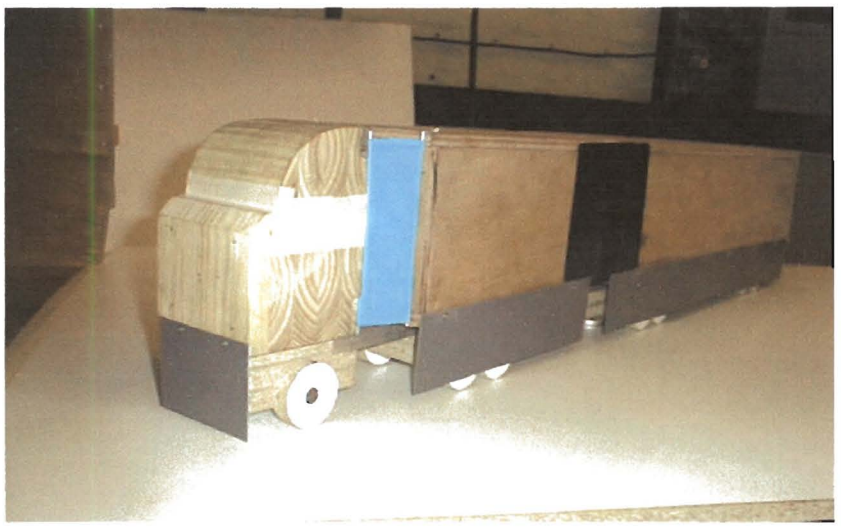

Figure B-6: Model with side gap seals, cab deflector and side skirts

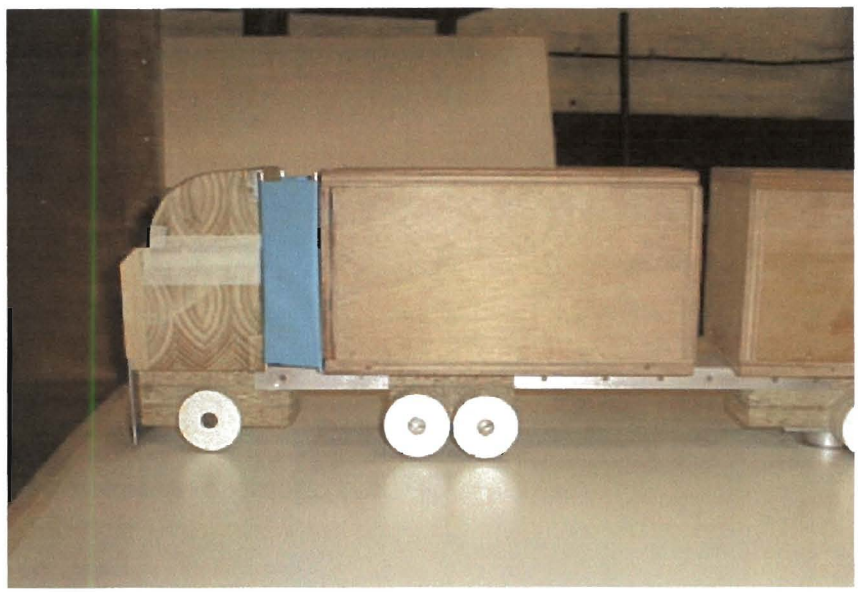

Figure B-7: Model with side gap seals

Figure B-8: Model with the cab deflector and side skirts

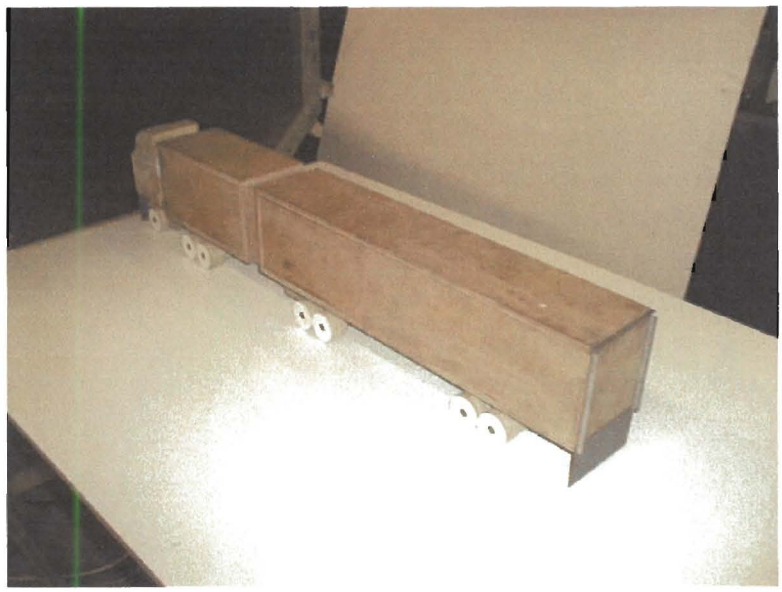

Figure B-9: Model mounted with rear fender and other devices

Figure B-10: Rear fender and rear cavities

Figure B-11: Edge fairings on the back of the rear trailer

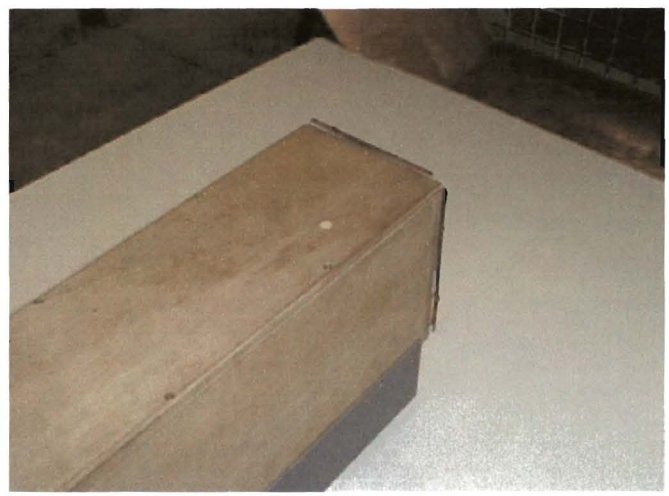

Figure B-12: Guide caves on the back of the rear trailer

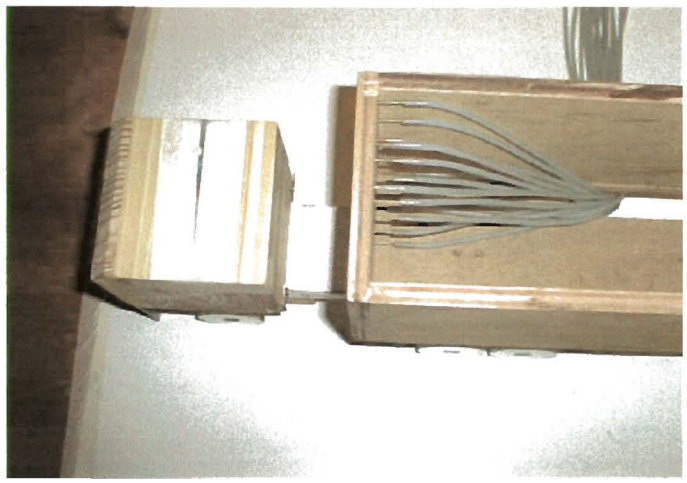

Figure B-13: Pressure tappings inside the front trailer

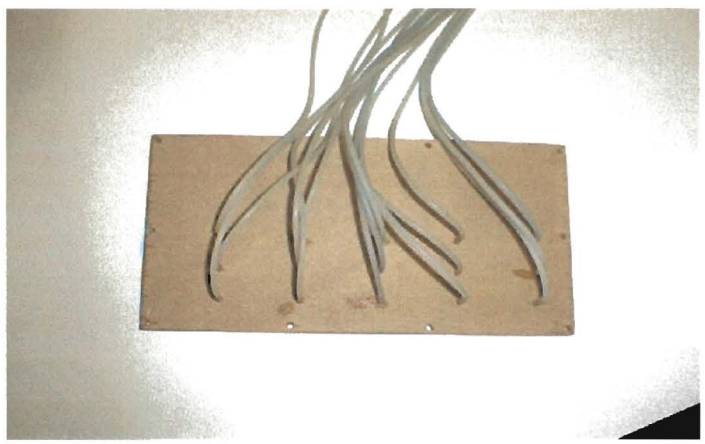

Figure B-14: Tappings on the top face of the front trailer

Figure B-15: Plastic tubes inside the rear trailer box

Figure B-16: Tappings on the top face of the rear trailer

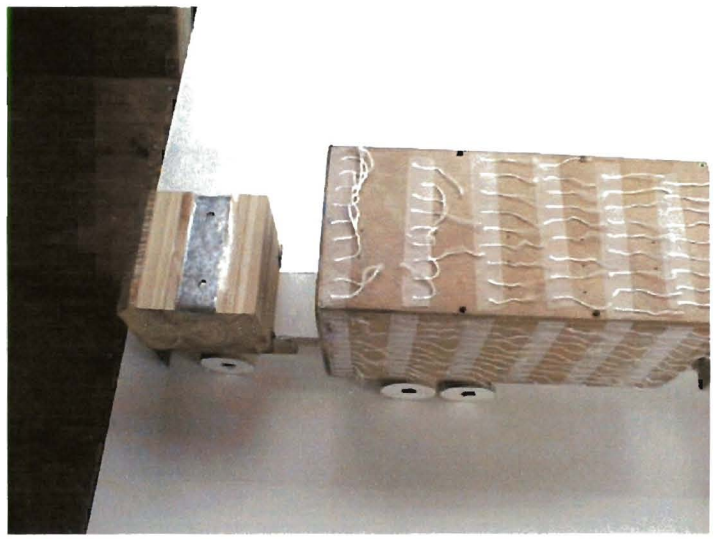

Figure B-17: Flow separation of the original model ($\beta = 0^0$)

Figure B-18: Flow separation of the original model ($\beta = 5^0$)

Figure B-19: No flow separation after adding the deflector

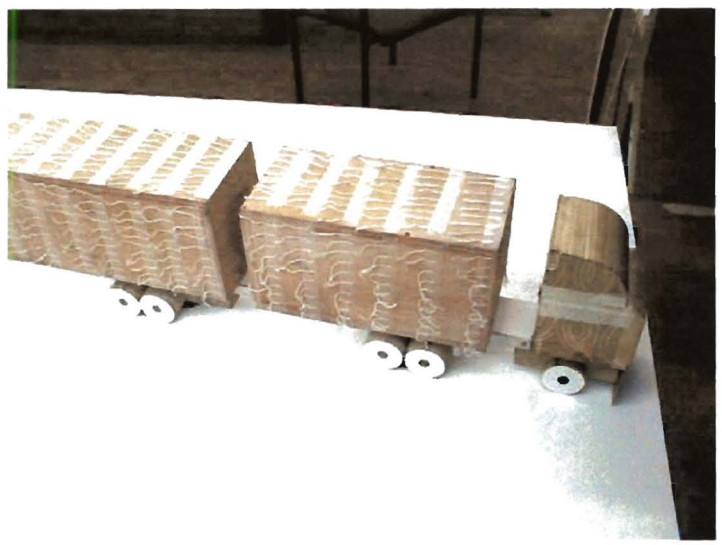

Figure B-20: Leeward side of the model with the deflector

Figure B-21:Top view of the model with side gap seals

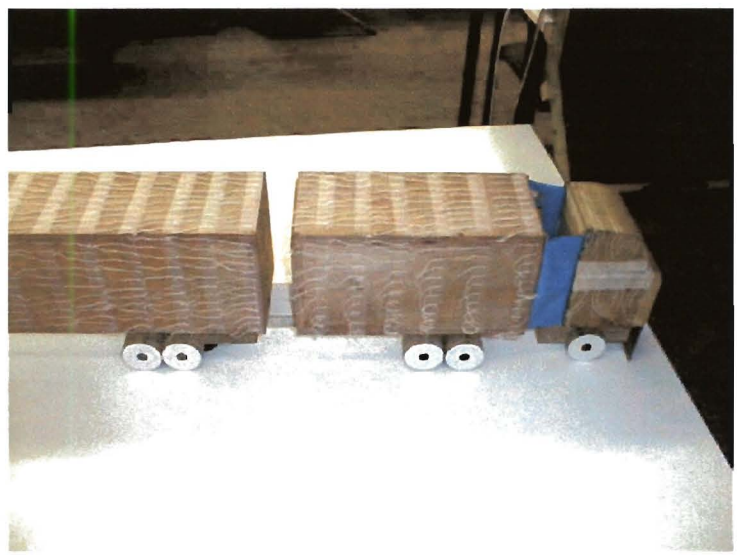

Figure B-22: Side view of the model with side gap seals

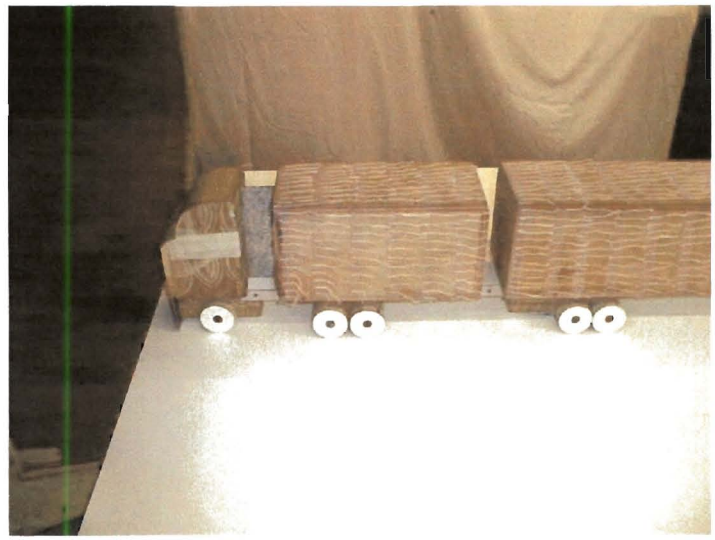

Figure B-23: The model with center gap seals ($\beta = 0^0$)

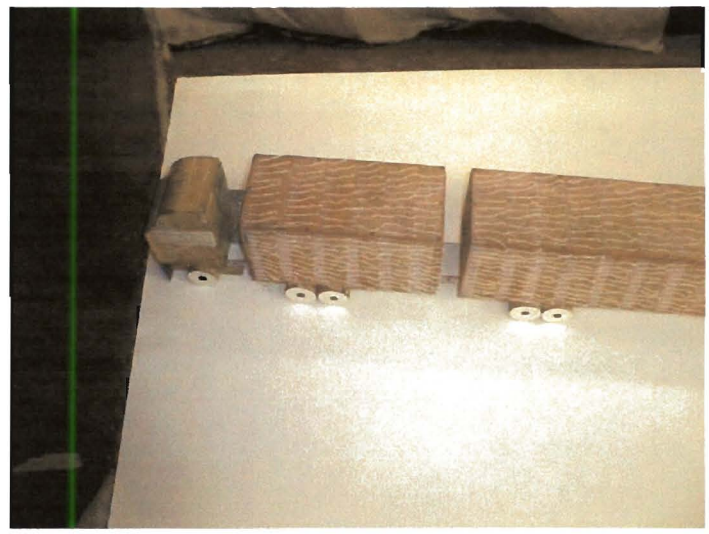

Figure B-24: The model with center gap seals ($\beta = 5^0$)

APPENDIX C – COMPUTATIONAL PROGRAMMES

The computational programs for the pre-processing and post-processing are presented in this appendix. Program No.1 includes the original model and models with a front fender, rear fender and rear cavity. Program No.2 is for the modes with a cab deflector and a combination of cab deflector and gap seal. The last program is a general post-processing program for all the models.

Program No.1

Pre-processing file

```
*******************************************************************************
// *** double trailer truck models : Flo++ input file
// *** To simulate airflow over the original truck model first
// *** Then do simulations for the models with front fender,
// *** rear fender and rear cavity separately
reset
// *** Mesh generation ****************************
#def Hc    0.16      m      height of the cab
#def Ht    0.215     m      height of the trailors
#def Lc    0.11      m       length of the cab
#def Ltr1  0.276     m      length of the trailor one
#def Ltr2  0.64      m      length of the trailor two
#def rho   1.205     kg/m^3  density of air
// *** Dimensions: 2.2 m in x-direction and 0.8 m in y-directions.
mcrea 0 0.3 15 0 0.8 40 0 0.01 1
view -1
plty hsurf
cp
bview 1                  //*** inlet boundary condition, V = 22 m/s
cset none
cgro 1
mcrea 0.3 1.8 150 0 0.4 40 0 0.01 1
cset none
cgro 2
mcrea 0.3 1.8 50 0.4 0.8 20 0 0.01 1
cset none
cgro 3
mcrea 1.8 2.2 16 0 0.8 40 0 0.01 1
```

```
view 3
cp
bview 2                  //*** outlet boundary condition.
cset none
cset all
save 3
resu 3
//*******Create embedded sets************************
escreate 1 15 2 601 1 751 1
repeat 19 1 15 0 300 0 300 0
//*******Create embedded sets************************
escreate 21 6601 3 6451 4 6452 4 6453 4
repeat 49 1 1 0 3 0 3 0 3 0
//*******Create embedded sets************************
escreate 71 7601 1 750 2 900 2
repeat 19 1 16 0 300 0 300 0
//***Check if embedded sets were  correctly defined**
cset none
cset eset
save 4
cset none
cset xyzr 0.4 0.51 0.05 0.17 0 0.01          //*** The tractor
cset xyzr 0.555 0.83 0.05 0.22 0 0.01        //*** The first trailer
cset xyzr 0.86 1.5 0.05 0.22 0 0.01          //*** The second trailer
cset xyzr 0.4 0.41 0.01 0.05 0 0.01          //*** The front fender
cset xyzr 1.49 1.5 0.01 0.05 0 0.01          //*** The rear fender
cset xyzr 1.5 1.52 0.21 0.22 0 0.01          //*** The rear cavity
cdel cset
cset none
cset all
view 0 0 1
cp
cnum off
cset none
cset all
#def vmx vmax
v vmx + 1 0.4 0.15 0             //*** triangle corner of the upper forward edge
v vmx + 2 0.4 0.15 0             //*** of cab
v vmx + 4 0.4 0.17 0
v vmx + 3 0.42 0.17 0
vcop 2 4 vran vmx + 1 vmax 1 0 0 0.01
cgro 5
c vmx + 1 vmx + 2 vmx + 3 vmx + 4 vmx + 5 vmx + 6 vmx + 7 vmx + 8
cset none
cset cgro 5
cgro 1
cref 2 2 1 cset
```

```
cset none
cset cgro 5
cdel cset
cset none
cset all
view 1 1 1
bzone 3 s                              //***other boundaries: wall and symmtry
bzone 3 n
bzone 4 b
bzone 4 f
// *** Fluid type definition *************************
turb on
tref 293
pref 100000 1
init stand 22 0 0
// *** Material properties and initial conditions ***
dens const rho
visc const 1.8e-5
// *** Cell and boundary group definitions ********
bgdef 1 inlet
0 22 0 0 1.205 0.001 0.001
bgdef 2 outlet
free 1
bgdef 3 wall
0 22 0 0
bgdef 4 symmetry
// *** Solution control ********************************
iter 1000 10
rela 0.7
conv 0.001
moni 1
cdis all,u              //***cell discretisation method: up wind.
walldata y
// *** Writing data for the solution stage **********
vmerge all
wmesh
wdef
screen reverse
// *** Save the modelling status ******************
save
view 0 0 1
plty wire
bp
*******************************************************************************
```

Program No.2

Pre-processing file

```
*******************************************************************************
// *** double trailer truck models: Flo++ input file
// *** simulation of the models with cab deflector and gap seals
reset
// *** Mesh generation ****************************
mcrea 0 0.3 15 0 0.8 40 0 0.01 1
view -1
plty hsurf
cp
bview 1
cset none
cgro 1
mcrea 0.3 1.8 150 0 0.4 40 0 0.01 1
cset none
cgro 2
mcrea 0.3 1.8 50 0.4 0.8 20 0 0.01 1
cset none
cgro 3
mcrea 1.8 2.2 16 0 0.8 40 0 0.01 1
view 3
cp
bview 2
cset none
cset all
plty hsurf
cnum on
save 3
resu 3
//*******Create embedded sets*************************
escreate 1 15 2 601 1 751 1
repeat 19 1 15 0 300 0 300 0
//*******Create embedded sets*************************
escreate 21 6601 3 6451 4 6452 4 6453 4
repeat 49 1 1 0 3 0 3 0 3 0
//*******Create embedded sets*************************
escreate 71 7601 1 750 2 900 2
repeat 19 1 16 0 300 0 300 0
//***Check if embedded sets were  correctly defined**
cset none
cset eset
save 4
cset none
```

```
cset xyzr 0.4 0.51 0.05 0.22 0 0.01
//cset xyzr 0.4 0.83 0.05 0.22 0 0.01      //*** WITHOUT GAP
cset xyzr 0.555 0.83 0.05 0.22 0 0.01
cset xyzr 0.86 1.5 0.05 0.22 0 0.01
cdel cset
cset none
cset all
view 0 0 1
cp
cset none
cset all
#def vmx vmax
v vmx + 1 0.4 0.15 0                    //*** cab roof deflector
v vmx + 2 0.4 0.15 0
v vmx + 4 0.4 0.22 0
v vmx + 3 0.48 0.22 0
vcop 2 4 vran vmx + 1 vmax 1 0 0 0.01
cgro 5
c vmx + 1 vmx + 2 vmx + 3 vmx + 4 vmx + 5 vmx + 6 vmx + 7 vmx + 8
cset none
cset cgro 5
cgro 1
cref 8 7 1 cset
cset none
cset cgro 5
cdel cset
cset none
cset all
view 1 1 1
bzone 3 s
bzone 3 n
bzone 4 b
bzone 4 f
cp
// *** Fluid type definition *************************
turb on
tref 293
pref 100000 1
init stand 22 0 0
// *** Material properties and initial conditions ***
dens const rho
visc const 1.8e-5
// *** Cell and boundary group definitions ********
bgdef 1 inlet
0 22 0 0 1.205 0.001 0.001
```

```
bgdef 2 outlet
free 1
bgdef 3 wall
0 22 0 0
bgdef 4 symmetry
// *** Solution control ********************************
iter 1000 10
rela 0.7
conv 0.001
moni 16
cdis all,u
walldata y
// *** Writing data for the solution stage **********
vmerge all
wmesh
wdef
screen reverse
// *** Save the modelling status *******************
save
view 0 0 1
plty hsurf
cp
*******************************************************************************
```

Program No.3

Post-processing file

```
*******************************************************************************
// ***doubl trailer truck models: Flo++ post-processing file
//***plot the air velocities and pressures on surfaces concerned
// ************************************************************
// *** Resume from the previous settings
resume
// *** Read the results
rresults
// *** Prepare a contour plot of magnitude velocity and pressure
pltype plane
ploption contou
view 0 0 1
vload p
cp
bload fpx                    //***Drag force in x-direction
cload m
ploption vector
cp
```

```
//***display pressure on the rear face of the rear trailer
cnum on
cset none
cset xyzr 1.5 1.51 0.05 0.22 0 0.01        //***the rear face of the rear trailer
pltype hsurf
ploption contou
cload p
view 2
cp
cload m
ploption contou
view 2
cp
//***display pressure on the front face of the front trailer
cset none
cset xyzr 0.545 0.555 0.05 0.22 0 0.01     //***the front face of the front trailer
pltype hsurf
ploption contou
cload p
view 0 0 0
cp
cload m
ploption contou
cp
//***display pressure on the front face of the trailor
cset none
cset xyzr 0.39 0.4 0.05 0.17 0 0.01        //***the front face of the tractor
pltype hsurf
cload p
view 2
cp
cload m
ploption contou
cp
cnum off
```